CHALMERS

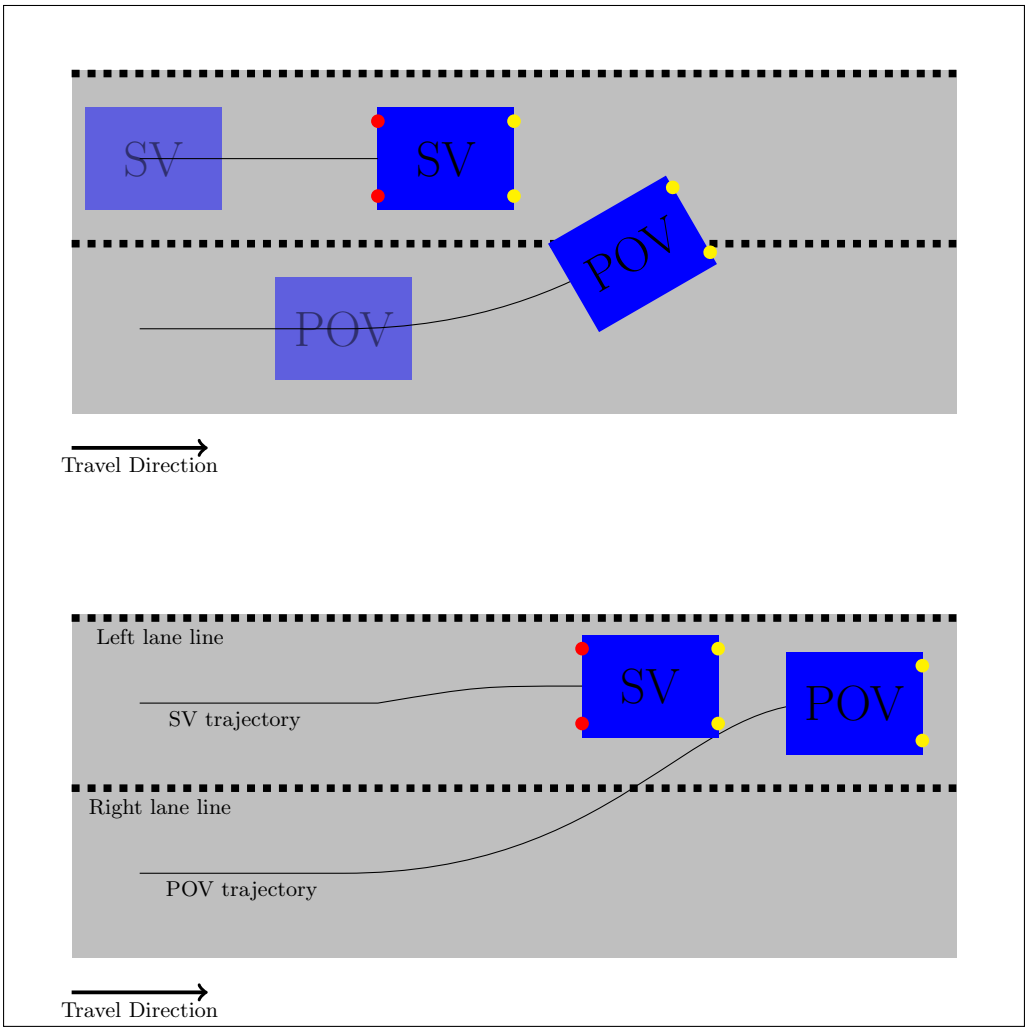

Statistical modelling of critical cut-ins for the evaluation of autonomous vehicles and advanced driver assistance systems

Master's thesis in Automotive Engineering

AHMED HAMDY SHAMS EL DIN

Department of Mechanics and Maritime Sciences
CHALMERS UNIVERSITY OF TECHNOLOGY
Göteborg, Sweden 2020

MASTER'S THESIS IN AUTOMOTIVE ENGINEERING

Statistical modelling of critical cut-ins for the evaluation of autonomous vehicles and advanced driver assistance systems

AHMED HAMDY SHAMS EL DIN

Department of Mechanics and Maritime Sciences
Division of Vehicle Safety
CHALMERS UNIVERSITY OF TECHNOLOGY

Göteborg, Sweden 2020

MASTER'S THESIS IN AUTOMOTIVE ENGINEERING

Statistical modelling of critical cut-ins for the evaluation of autonomous vehicles and advanced driver assistance systems

AHMED HAMDY SHAMS EL DIN

Department of Mechanics and Maritime Sciences
Division of Vehicle Safety
CHALMERS UNIVERSITY OF TECHNOLOGY

Göteborg, Sweden 2020

Statistical modelling of critical cut-ins for the evaluation of autonomous vehicles and advanced driver assistance systems
AHMED HAMDY SHAMS EL DIN

- Examiner: Jonas Bärgman
  Associate Professor, Division of Vehicle Safety
  Department of Mechanics and Maritime Sciences
  Chalmers University of Technology
  jonas@barman@chalmers.se
- Academic Supervisor: Giulio Bianchi Piccinini
  Associate Professor, Division of Vehicle Safety
  Department of Mechanics and Maritime Sciences
  Chalmers University of Technology
  giulio.piccinini@chalmers.se
- Industry Supervisor: Majid Khorsand Vakilzadeh
  Data scientist
  Zenuity
  majid.vakilzadeh@zenuity.com

Master's thesis 2020:22
Department of Mechanics and Maritime Sciences
Division of Vehicle Safety
Chalmers University of Technology
SE-412 96 Göteborg
Sweden
Telephone: +46 (0)31-772 1000

Chalmers Reproservice
Göteborg, Sweden 2020

Statistical modelling of critical cut-ins for the evaluation of autonomous vehicles and advanced driver assistance systems
Master's thesis in Automotive Engineering
AHMED HAMDY SHAMS EL DIN
Department of Mechanics and Maritime Sciences
Division of Vehicle Safety
Chalmers University of Technology

Abstract

Understanding human behaviour in traffic is an integral part of developing active safety systems (ADAS) and autonomous vehicles (AV). Such systems require rigorous testing before they can be put in commercial use. This thesis aimed to study data collected as part of the second Strategic Highway Research Program (SHRP2) Naturalistic Driving Study (NDS) to improve the estimation made in the tails of a driver model for lane changing. This was to be done through annotating a data-set of 1191 critical lane-change events provided through SHRP2 NDS. Annotation was done using an annotation tool that was developed for this purpose as part of a previous project. The trajectories of the manoeuvres were then extracted and parameterised using ridge regression. It was found that 86 of the 1191 events were suitable for annotation. Due to the limited quality of the data and number of usable events, the thesis aim was redirected to model the uncertainty of the annotation method using 9 events annotated by 5 annotators. Two linear regression models were then developed to estimate the uncertainty of this annotation method. The results show that the models can predict the uncertainty based on the limited number of events that were available. These results have potential to be used to estimate the uncertainty of the parameterised trajectories in future work.

Keywords: Statistical modelling, ADAS, AV, Driver models, Naturalistic Driving Data, Lane changes, Near-crashes, Linear Regression

Acknowledgements

This thesis was carried out jointly at Chalmers University of Technology and Zenuity

Firstly, I would like to express sincere my gratitude to my supervisors Giulio Piccinini and Majid Khorsand, as well as my examiner Jonas Bärgman who have all contributed with their valuable time and knowledge to make the outcome of thesis thesis possible.

I would also like to thank Pierluigi Olleja for showing interest in this thesis from the start and supporting the annotation process when it was needed.

And of course, I am obliged to thank Mohamed Takkoush for playing a key roll in making this thesis possible.

Finally, I would like to thank all friends and family whom have supported me throughout my studies and refuelled my motivation when needed.

This work has been performed under the VTTI Data License Agreement (SHRP2-DUL-A-3-19-432). The findings and conclusions of this report are those of the author(s) and do not necessarily represent the views of VTTI, the Transportation Research Board, or the National Academies

Contents

Glossary

ADAS Advanced Driver Assistance System. 1, 2, 3, 4, 5, 49

AEBS Automatic Emergency Braking System. 1, 4

AV Autonomous Vehicle. 1, 2, 3, 4, 5, 49

CAN Controller Area Network. 7, 18, 27, 31

DAS Data Acquisition System. 7, 14

EuroNCAP European New Car Assessment Programme. 1

FOT Field Operation Test. 3, 5, 49

GUI Graphical User Interface. 11, 49

MV Manually driven Vehicle. 1

NDS Naturalistic Driving Study. 3, 4, 5, 7, 48

POV Principle Other Vehicle. viii, 4, 5, 7, 8, 10, 11, 12, 14, 15, 16, 18, 19, 20, 21, 24, 27, 28, 31, 32, 33, 34, 37, 39, 41, 43, 44, 45, 48, 49, 50

SAE Society of Automotive Engineers. 1

SAFER Vehicle and Traffic Safety Center at Chalmers. 16

SHRP2 second Strategic Highway Research Program. 5, 7, 11, 14, 48

SV Subject Vehicle. viii, 4, 5, 7, 8, 9, 10, 12, 15, 16, 17, 18, 19, 26, 27, 28, 31, 32, 33, 34, 39, 41, 43, 45, 49

TTC Time To Collision. 3, 29

VTTI Virginia Tech Transportation Institute. 7, 28

List of Figures

List of Tables

1 Introduction

Modern automotive manufacturers have in the past few decades striven to automate driver functions wherever possible and plan a radical revision of the driver's role [1]. Even though humans are regarded to be very good drivers, studies have shown that two thirds of accidents are mainly caused by human error and that this factor is present in 90% of accidents [2]. The aim of automating the driving tasks is to reduce human error, and thereby target the largest contributor to traffic accidents. Advanced Driver Assistance Systems (ADAS) work to avoid accidents by constantly monitoring the driving environment and take action in safety critical scenarios. The safety gain attributed to (ADAS) is apparent as the European New Car Assessment Programme (EuroNCAP) has introduced a test for Automatic Emergency Braking System (AEBS) that has become a part of the safety rating of modern cars. The introduction of such tests was believed to accelerate penetration of ADAS in Europe [3]. As a result, the automotive industry is now closer than ever to achieve the goal of a truly autonomous vehicle, although there are still many hurdles to overcome in this pursuit.

The Society of Automotive Engineers (SAE) has defined six levels of automation ranging between level 0 and level 5. As seen in in table 1.1, the automation level is gradually increased where levels 1,2 and 3 represent driving assistance systems that can assist the driver with certain tasks in certain scenarios [4]. Level 4 is high automation, where the system can handle most driving tasks in most scenarios. Such systems should also function even if a human driver does not respond to a request for intervention. Level 5 is full automation where the human driver does not need to monitor the driving task in all driving conditions and scenarios [5].

Most commercially available ADAS today are still considered to be on SAE level 2, meaning that they require constant human supervision. From SAE level 3 on-wards, there is a part of the driving task that the human driver does not need to monitor and the driver should only intervene when a take-over request is sent by the system. This raises the question about who will be held accountable if a crash happens, the manufacturer or the driver? This topic cannot be discussed without raising several legal and ethical concerns and it is not the aim of this project. However, it underlines the relevance of the development of safe Autonomous Vehicles (AV) by the manufacturers. Then, it is reasonable to assume that AVs will be developed to be "perfect drivers", following all traffic rules and minimising risk-taking while making decisions. Since AVs are programmed, their behaviour should be also predictable by other vehicles of their kind. However, since the automobile has a life span of around 30 years, it is assumed that the first AVs will have to operate in traffic around older, Manually driven Vehicles (MV) [6]. Research on this topic has been conducted before and focused on how AVs would communicate with MVs and other road users [7]. The takeaway is that AV should be able to detect potentially dangerous behaviour of MVs in it surrounding, and act upon this detection to evade critical scenarios.

SAE level	Description
Level 0: No Automation	The human driver is doing all aspects of the driving task
Level 1: Driver Assistance	Systems that sometimes assist the driver with a certain driving task, such as lateral or longitudinal
Level 2: Partial Automation	Systems that perform a task, such as lateral and longitudinal control. The human driver monitors and is otherwise responsible for remainder of driving tasks
Level 3: Conditional Automation	Systems that manage all driving tasks and monitor the driving environment in certain driving conditions. The human driver only intervenes when the system requires assistance
Level 4: High Automation	Systems that drives and monitors in certain environments and conditions without supervision. Such systems are considered fully autonomous for most driving scenarios
Level 5: Full Automation	Systems that do everything a human driver could do under all conditions while matching or exceeding human capabilities

Table 1.1: The SAE six levels of automation [4]

Predicting human behaviour in traffic is not an easy task and researchers have for many years developed computational human driver models to describe human behaviour in different scenarios. The scenario that was studied in this work is represented by critical lane changes as illustrated in figure 1.1, where the lead vehicle, referred to as Principle Other Vehicle (POV), changes lane or cuts in front of the follow vehicle, referred to as Subject Vehicle (SV).

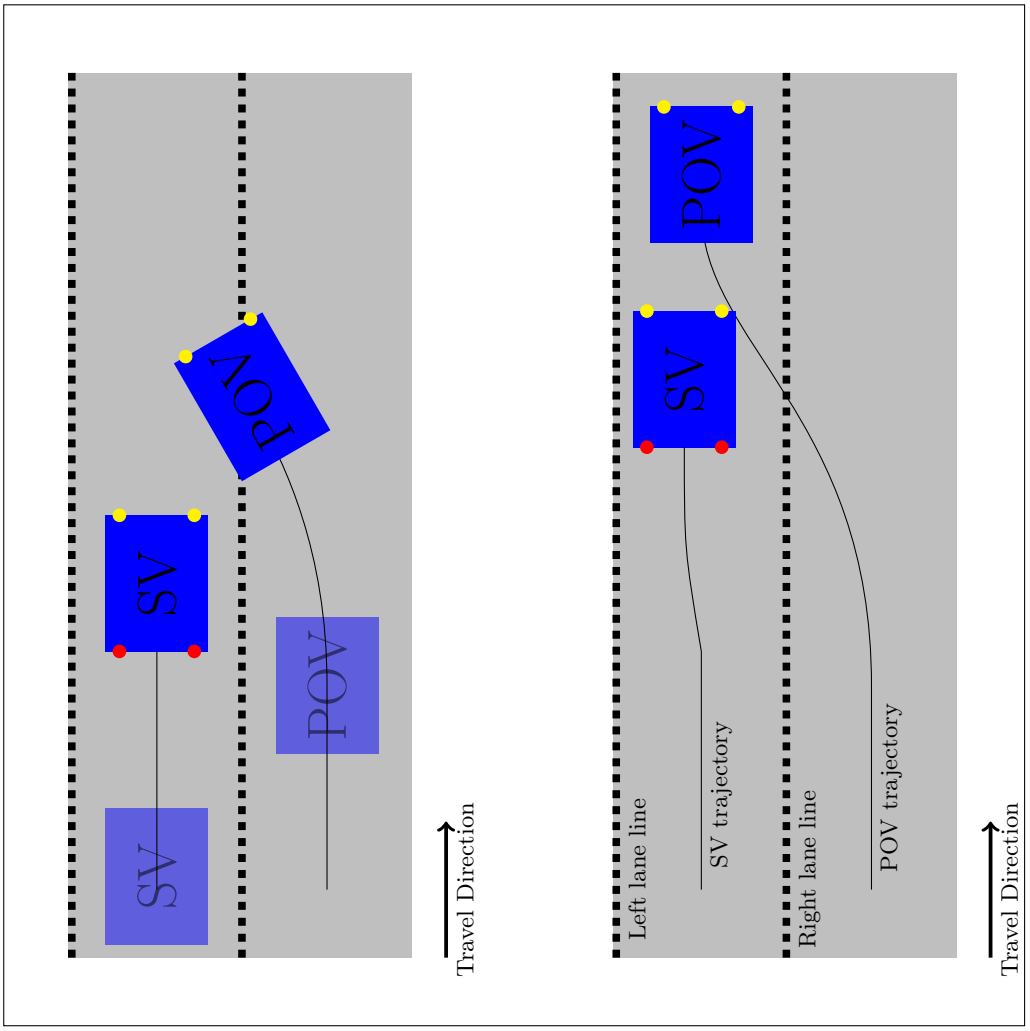

Figure 1.1: *Cut in scenario considered for this work*

1.1 Background

Lane changes are common manoeuvres that can cause substantial impact on traffic flow, as previous studies have shown that lane changing tends to cause negative shock waves in traffic and may lead to severe crashes [8]. According to a study conducted using accident data from 1991 in the United States of America (USA), about 4% of all crashes were attributed to lane change/merge manoeuvres, which represented 244000 crashes [9]. The study also states that approximately 386000 lane change/merge crashes went unreported. Totally, these accounted for 10% crash-caused delay that same year. These numbers show the importance of properly studying such events and work on preventing them using ADAS and AV technology. Before an ADAS or AV function can be put into commercial use, they have to be tested rigorously to ensure operational safety.

There are different methods of testing such systems. One method is though using Field Operation Tests (FOT), where a number of instrumented vehicles drive in a test setting or on regular roads. As these vehicles drive, they collect data that can later be studied to evaluate the safety gain of such systems. Even though

this method provides high quality data, it is restricted since there are very few crashes and critical events in the data-set, as was shown by the EuroFOT large scale operation test using hundreds of equipped vehicles [10]. For safety evaluation, it is important to have data from critical events since they provide an insight of what leads to a crash. This makes this method of evaluation both costly and time consuming. To compensate for the lack of crashes, near-crashes are often used as surrogate events, assuming that preventing near-crashes should also mean that real crashes are prevented [11].

A different approach to test ADAS is to do part of the evaluation using computer simulations. This approach allows for better control over the conditions that one wishes to test and ensures both time and cost efficiency [12]. However, simulation results are only satisfactory if the models used for the simulations are reliable. This includes modelling of the ADAS function, traffic environment, vehicle and driver [13].

This project focuses on driver modelling in critical cut-ins. A driver model aims to estimate the behaviour of a driver in a specific scenario. To develop and evaluate such models, data about how drivers behave in traffic is needed. Mathematical models are then used to recreate such behaviour in simulations [14]. There are several ways to gather data about driver behaviour. The aforementioned FOT is one, but as previously mentioned, critical events are rare in traffic and gathering enough of them is challenging using FOT. Accident databases are another source of data, however, accident databases contain very basic information about the accident, such as vehicle specifications, impact speed derived from vehicle deformation, collision type, a description of the environment at the accident site and potential injuries or fatalities [15]. Such databases have been used to study the impact of ADAS functions in the past [16]. However, for the development of driver models, more data is needed about the pre-crash phase such as vehicle telemetry data. Another source of data is Naturalistic Driver Studies (NDS). In such studies, regular drivers have their vehicles instrumented with computers, radars and cameras. They then drive their regular vehicles in "naturalistic conditions" while the instrumentation is gathering data. This allows faster and more cost efficient collection of near-crashes compared to FOT; since there are more vehicles gathering data; and better data about the pre-crash phase compared to accident data bases [11]. It is therefore suitable as a data source for the development of driver models for certain scenarios.

1.2 Literature Review

Lane change behaviour has been studied in the past with different methods and approaches. The purpose of this review is to research how driving data is used to set criteria for active safety features, how lane-change behaviour is modelled, how traffic simulations have been used to evaluate the safety benefit of active safety features and if the approach taken in this project is found in previous work. The findings are presented in this section.

1.2.1 Driving data for ADAS development

Studying driver behaviour in general is an integral part of developing an ADAS function. Lee, Olsen, Wierwille, et al. [17] used two highly equipped research vehicles driven by 16 commuters who drove each vehicle for a period of 10 days, to record data. A total of 8667 lane-changes were collected, 91% of which were found uneventful. The experimental design included three variables being gender, route (interstate or highway) and vehicle type (SUV or sedan). Lane-changes were split into different categories of urgency and severity. Urgency was rated on a 4-point scale (1= not urgent, 4 = critical) indicating how soon the lane change was needed based on the Time To Collision (TTC) with the closest vehicle ahead or behind if the follow vehicle is accelerating. Severity was rated on a 7-point scale (1=no conflict , 7=physical contact), indicating the degree to which the vehicle in the destination lane was cut off based on the proximity of the said vehicle to the vehicle changing lane. The values for all these variables were determined using an annotation tool that, given the video file and recorded telemetry data, provided an archive of the complete event suitable for later analysis. The results were used to provide recommendations for designers of Collision Avoidance Systems (CAS).

Kauffmann et al. [18] used a full scale driving simulator to investigate the drivers' perceived cooperation of AVs in lane-changes. A group of 25 drivers were asked to drive in the driving simulator and exposed to different cut-in manoeuvres by a leading AV in the adjacent lane. Three variables - being start indicator signal (12m, 16m 20m), wait-time (1s, 2s, 3s) and lane-change duration (4s, 6s, 8s) - were used to describe a cut-in. After

the drivers had been subjected to the same combination of cut-ins, they were asked to fill in a questionnaire to rate the perceived willingness to cooperate, unambiguity and criticality of the merging AV. An Analysis Of Variance (ANOVA) was conducted on start indicator signal, wait-time and lane change duration to investigate their influence on the perceived cooperation of the AV. It was concluded from the results that a cut-in was perceived more cooperative when the av started the indicator signal at a 20$[m]$ distance from the following vehicle, while wait-time and lane-change duration had less significance on the results. The paper concluded with stating two limitation of this study. First, the relatively limited time in the simulating environment could limit the generalizability of the results. Second, the artificial environment that was used in this study could not capture several factors that the driver would be exposed to in real life and that may lead to more complex decisions. Despite these limitations, this study provided an indication on how automated systems could be developed to be perceived more cooperative by surrounding drivers.

1.2.2 Modelling of Lane-change Behaviour

The first attempts to model lane-change behaviour were mainly done to conduct capacity analysis and safety studies of road infrastructures. Gipps [19] introduced the first lane-changing model developed for highway driving using data gathered from a 2000m highway section with intersections, off-ramps and obstructions in some lanes. Toledo, Koutsopoulos, and Ben-Akiva [20] found that the Gipps model had limitations, such as neglecting variations between drivers and the inconsistencies in the behaviour of a driver over time. A different model was then proposed using data gathered in a similar manner from a highway section. The purpose was to capture how the choice of target lane on a highway affects the gap acceptance of drivers during lane-changes. The proposed model could be used for traffic simulations to evaluate traffic flow characteristics.

More recent work has developed models to be used in simulations for safety evaluation of ADAS functions. Zhao et al. [21] used data gathered though NDS to model safety-critical lane-changes and recreate these events in simulations to test an AEBS function. The NDS dataset was recorded using 2842 vehicles over a period of two years. Lane-changes were identified using the following criteria:

- $v_{pov}(t_{LC}) \in (2m/s, 40m/s)$
- $v_{sv}(t_{LC}) \in (2m/s, 40m/s)$
- $R_{pov}(t_{LC}) \in (0.1m, 75m)$
- $\dot{R}_{pov} < 0m/s$

where v_{pov} is POV speed, v_{sv} is SV speed, R_{pov} is SV range to POV and t_{LC} is time of POV lane cross. Using these criteria, 173 692 lane-changes were identified.

Gap acceptance was then evaluated using $R_{pov}(t_{LC})$, $v_{sv}(t_{LC})$ and Time To Collision $TTC_{pov}(t_{LC})$. Higher $R_{pov}(t_{LC})$ and $TTC_{pov}(t_{LC})$ values indicated safer lane-changes. Statistical analysis was done for these R_{pov} and TTC_{pov} for low, medium and high v_{sv} ranges and two models were developed to estimate $R_{pov}(t_{LC})$ and $TTC_{pov}(t_{LC})$ respectively for different $v_{sv}(t_{LC})$ values. These models were then used in simulations to estimate lane-change conflict, crash and injury rates of a given AV, from 2000 to 20000 times faster in simulations compared to relying only on NDS data. This proved the advantage of using simulations for evaluating safety benefit of AV and ADAS functions.

A similar approach was taken by Wang, Yang, and Hurwitz [22] using data gathered in Shanghai Naturalistic Driving Study (SH-NDS). The purpose was to model lane-changing behaviour of drivers specifically in China. It was stated that drivers in China performed lane-changes nearly three times more often compared to the U.S, due to the challenging driving environment originated by omnipresent pedestrians, electric bikes, bicycles and aggressive drivers. This raised concerns about the potential unsuitability of simulations and ADAS functions in China, as the ADAS algorithms are calibrated using data from different countries. An extraction algorithm was developed to obtain cut-in events using radar's lateral and longitudinal ranges, position in the lane, lateral acceleration and vehicle speed, all of which were recorded by the SV. The obtained events were those where the SV stayed in its lane during the entire manoeuvre. The extracted events were then manually validated by observing the videos from the forward roadway camera. The following three critical time points were found in the cut-in manoeuvre:

- Initiation point: Local maximum of Y_{pov}
- Cross-lane point: When Y_{pov} has decreased to less than the lane edge
- Stabilisation: The first zero value of Y_{pov}

Where Y_{pov} is the SV lateral range to POV. A total of 5608 cut-ins were identified. Through viewing the video from the forward roadway camera for these events, the following 6 independent variables were defined:

- Environmental factors
  - Traffic density (hight, low, medium)
  - Weather (rainy, sunny)
  - Light conditions (night time, Day time)
- Kinematic parameters
  - Vehicle type (heavy, light)
  - Relative speed between SV and POV
  - Acceleration

These were then studied to model cut-in gap acceptance using a three-level mixed effects linear regression model.

1.2.3 Problem Formulation and Aim

It is apparent that lane-change modelling is a well studied subject. However, little research was found about recreating the trajectory of the POV during the manoeuvre. Zhao et al. [21] used the distributions of the range $R_{pov}(t_{LC})$ and time to collision $TTC_{pov}(T_{LC})$ for three speed ranges to extend the data-set for all speed ranges. Wang, Yang, and Hurwitz [22] used the lane-change event to annotate different independent variables. These variables were then used to model the lane-change behaviour through predicting the longitudinal lead and lag gaps of the POV given different inputs of the defined variables.

More recent work has attempted to develop a statistical lane-change model using not only the lead and lag gaps, but also the full lateral and longitudinal trajectories of the POV. However, such models are based on FOT collected data with a limited number of critical events. This means that there is not enough data to model the safety-critical lane changes which can be assumed to represent the tails of a normal distribution as illustrated in 1.2. Instead, the tails are estimated through extending the model using the non-critical events that were collected, as a surrogate for critical events. Improving the estimation of such models is essential for traffic safety simulations aiming to evaluate the safety of AV and ADAS.

Then, the aim of this thesis is to evaluate the estimation of the tails of statistical models of this kind. For reaching the aim, cut-in manoeuvres that resulted in near-crashes were studied. The data-set used for this was provided through second Strategic Highway Research Program (SHRP2) NDS, accessed at SAFER (Vehicle and Traffic Safety Centre by Chalmers). The goal was to use an annotation tool that was developed for this purpose in a previous project to extract the trajectory of the POV during the manoeuvre, as described in detail in El Din et al. [23]. Only completed lane changes were considered for this model. During the work, the aim had to be redefined, due to limited number of events that could be used. This outcome derived from the reduced access to the annotation rooms located at SAFER, as a consequence of the covid-19 outbreak. Therefore, the scope of the thesis was redirected to model the uncertainty of the tool output; using a number of events annotated by several annotators; and determine if this method of annotation is suitable for the statistical analysis. Nevertheless, the preparation for the statistical modelling was included in the thesis, as a valuable input for future work on this subject.

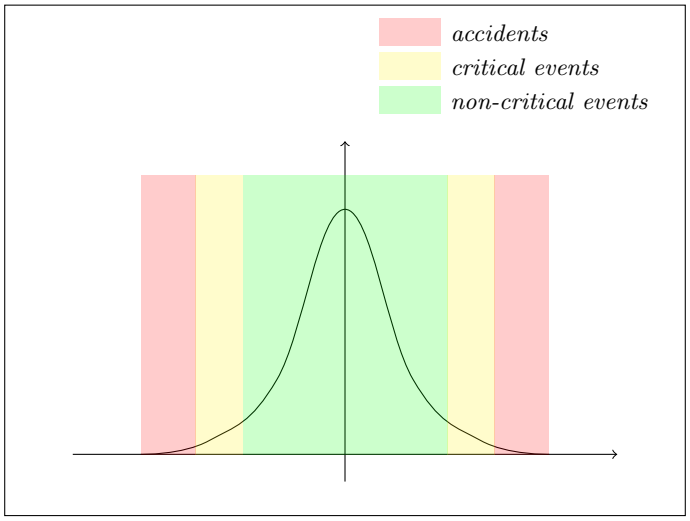

Figure 1.2: *Generalised distribution of all events that occur in traffic where critical events are near the tails of the distribution*

2 Methodology

The purpose of the methodology is to explain how the uncertainty model was obtained, starting from the raw data. The methodology is described in different sections. First, the preparation of the data and identification of relevant events. Then, how the annotation was done and what output variables and model parameters were obtained. Then how these variables and model parameters were used to describe the POV and SV trajectories during the manoeuvre in preparation for statistical modelling of the lane change manoeuvre. Last is a description of how an uncertainty model based on the data from the tool output was developed.

2.1 Pre-processing Data

The second Strategic Highway Research Program (SHRP2) initiated the largest Naturalistic Driving Study (NDS) of its kind with nearly 2360 participants as of September 2012, where the Virginia Tech Transportation Institute (VTTI) served as the technical coordinator and study design contractor [24]. The goal was to address the role of driver performance and behaviour in traffic safety. This study was conducted in six sites in the United States with 150 to 450 participating vehicles in each site. The purpose was to understand how the driver interacts and adapts to changing driving conditions such as traffic environment, roadway characteristics, traffic control devices and other environmental features. The study also aimed to assess the changes in collision risk associated with each of these variables [25].

Participants went to specified field contractor's installations facility to have their vehicles instrumented with the Data Acquisition System (DAS) which included a forward mounted radar, forward roadway camera, rear roadway camera, rear camera, head tracking unit OBD connector and GPS antenna [24]. By the end of the study, a total of 50 million miles of travel were collected [26].

A total of 1191 SHRP2 critical lane-change events were provided from VTTI for this project after a request made by Chalmers researchers and Zenuity. Assuming that these 1191 are all critical lane-changes collected in the SHRP2 data-set, the exposure to this type of event can be estimated through dividing the number of events by the total number of collected miles of travel in the full data-set as $1191/50 \approx 2.8[events/million\ miles]$. This data-set was viewed inside access controlled secure rooms, where the video was not visible from outside of the rooms. Only completed lane changes that resulted in near crashes would be considered for this model. These are the cases where the POV does a full lane change in-front of the SV, where the SV stayed in its lane during the entire manoeuvre. These criteria were set as a result of the problem description.

2.1.1 Converting data format and Re-structuring data

All events provided in the data-set were crashes or near crashes that resulted from cut-in events. For each event, a '.csv' file was delivered with time-series data that included the radar ranges, SV speed and several other signals measured form the Controller Area Network (CAN) of the SV. There was also segmented information describing the event itself in text including locality, vehicle type and manoeuvre type, that was provided in a separate '.csv' file. For each event a '.mp4' video was also provided from the forward-roadway camera (dash cam) sampled at $15Hz$ for a duration of $30[s]$ giving a total number of $450[frames]$ in each video file. These files were used to make '.mat' files using MATLAB, since this was the format that is compatible with the annotation tool and other tools at SAFER.

Upon analysing the first few events, a synchronisation issue was found with the data: the video and the time-series data were the same duration of $30[s]$ but had a time offset which was different for different events, as illustrated in figure 2.1. For some events, the video footage started earlier than the time-series data. This offset was observed when manually comparing the time stamp printed on the first video frame and the first time stamp in the time-series data. This meant that the tool output and the time-series data were not synchronised. This issue was presented to VTTI which provided a solution on the form of '.cvs' file containing the timestamp of the first video frame for all events. Using this information, the offset between the time-series data and the forward roadway footage was calculated and the video and the time-series data could be synchronised.

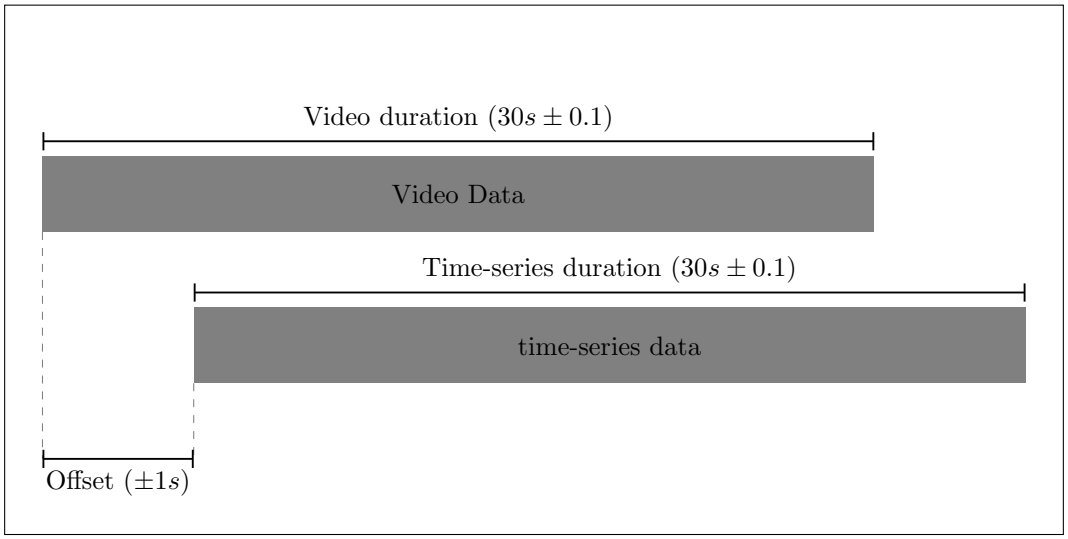

Figure 2.1: *Illustration of synchronization issue*

2.1.2 Identification of relevant events

All events in the data-set were crashes and near crashes as a result of critical cut-in manoeuvres. Overall, the data-set included 9 crashes and 1182 near-crashes but not all events were suitable for annotation. As described earlier, the scope of this thesis has been limited to studying critical cut-in manoeuvres where: a) the event severity is near crash; b) the POV is a passenger vehicle (i.e. not a truck); c) the POV does a complete lane change, meaning that partial (incompleted) lane-changes are not considered; d) the manoeuvre occurred on an interstate or highway; and e) the SV stayed in its lane during the entire manoeuvre.

Apart from the definition of the problem, also some limitations of the methodology restricted the number of events suitable for annotation. The first limitation was that for the annotation to be possible, the POV had to be visible in the video frame at all time during the manoeuvre. In practice, this occurred when the entire length of the POV was ahead of the SV at the beginning of the manoeuvre. After analysing a number of events, it was found that this criterion was met for most events where the incident type was *'Rear-end'*. On the other hand, this criterion was not satisfied for other incident types such as *'Side-swipe'*. Therefore only events where the SHRP2 variable *'IncidentType1'* was coded as *'Rear-end'* were chosen for annotation. The number of the events in the data-set for each category of the variable *'IncidentType1'* is reported in Table 2.1.

Incident Type	Occurrences
Sideswipe	653
Rear-end	532
Backing into traffic	6

Table 2.1: The different incident types that were found in the data-set and their occurrences

Road type was also a limitation, since some events occurred on roads without any lane markings, such as parking spaces and on play grounds. The type of road was classified in the data-set according to different categories of the variable *'Locality'*. The categories and their occurrences are shown in figure 2.2.

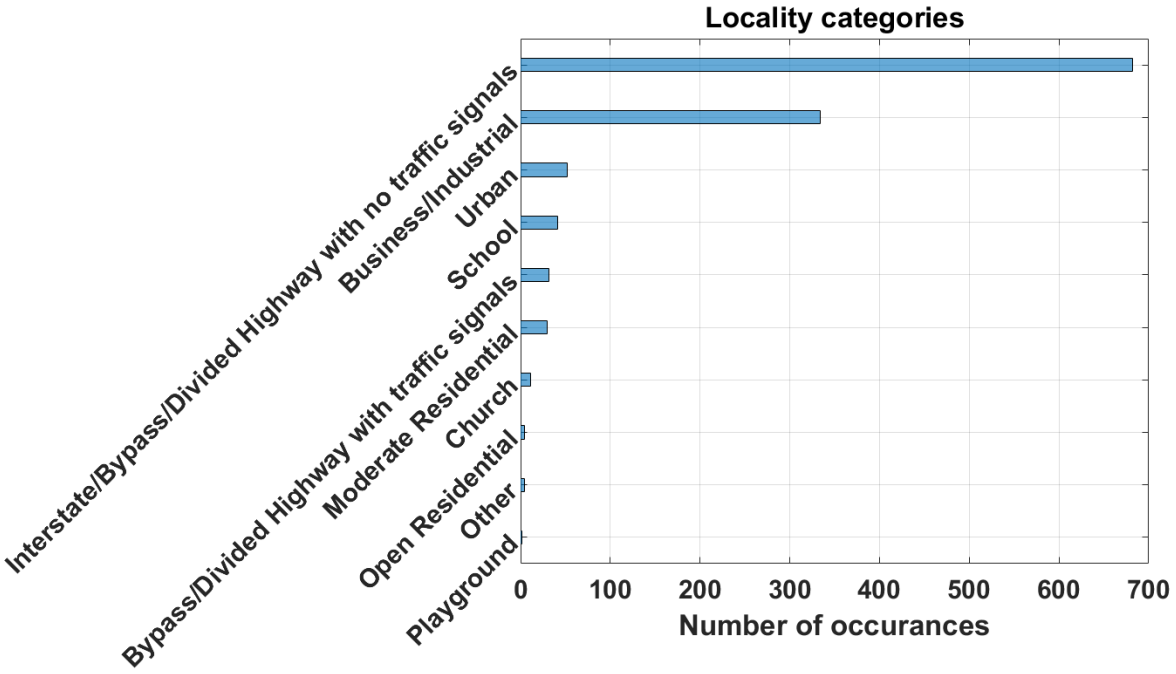

Figure 2.2: *Distribution of events according to the categories of the variable 'Locality', in the data-set*

Only the events where the locality included *'Highway'* were considered. The choice was motivated by the need to have lane-markings visible for most part of the recording, which was often true for events that occurred on a highway.

There was also a variable called *'PreIncidentManouver'* that described the state of the SV just before the start of the manoeuvre. For this variable, the distribution of the different categories is reported in figure 2.3.

Only the events where the *'PreIncidentManouver'* was *'Going straight, constant speed'* and *'Going straight, accelerating'* were chosen for annotation. This choice was meant that the SV should be in the same lane during the entire manoeuvre.

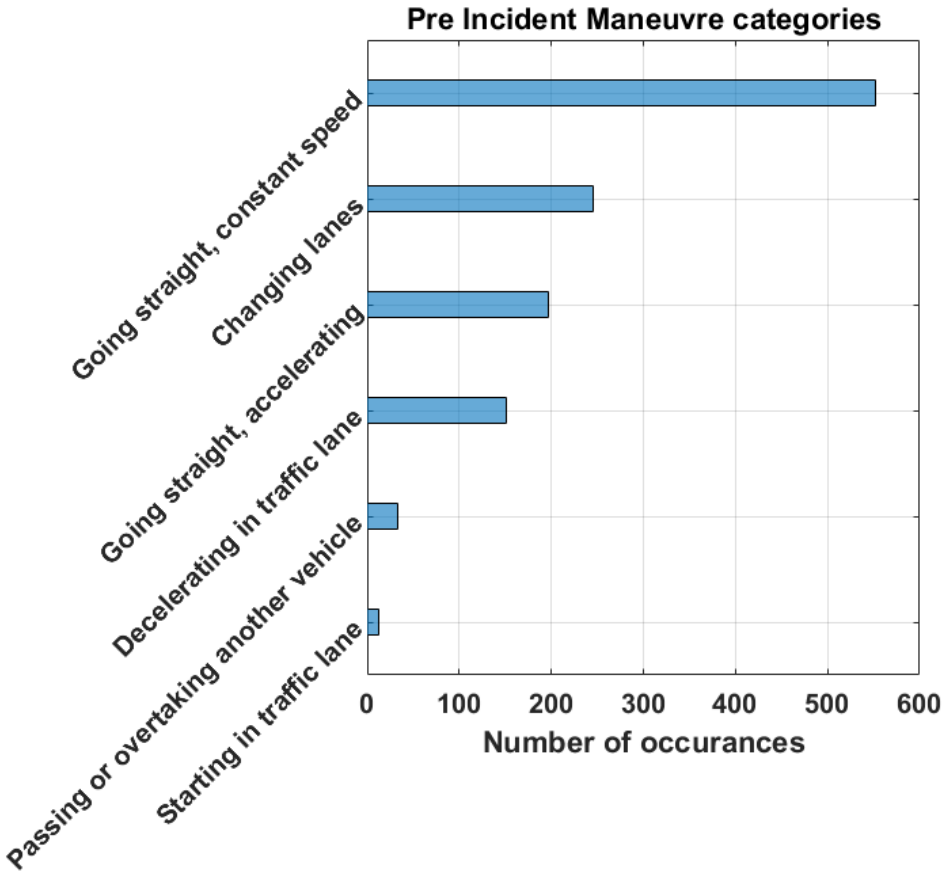

Figure 2.3: *Distribution of events according to the categories of the variable 'PreIncidentManouver' in the data-set*

To summarise, the following conditions were required for an event to be considered for annotation:

- Event severity is *'Near-crash'* as a it was intended to model lane-change manoeuvres in critical scenarios, as was set in the problem description in this project.
- Locality invcludes *'Highway'*, partly due to the problem description and to also assure that the lane markings are visible.
- Incident type is *'Rear-end'* to assure that the POV is in the video frame during the entire manoeuvre.
- Pre-incident manoeuvre is *'Going straight'* to assure that the SV is travelling in the same lane during the event.

Apart from these limitations, events could also be discarded during the annotation process if other issues existed such as: POV is out of image frame or the POV performs a partial lane change. In such a case, the annotator had the ability to exclude it and specify a reason in written text for its exclusion.

2.2 Annotation of Data

In this section, the annotation tool is described in detail. First is a short overview of the Graphical User Interface (GUI) of the tool. Then, the different steps of the annotation process are presented. Finally, a summary of the improvements that were made to the original tool to improve usability and accuracy for this thesis and future projects.

2.2.1 Annotation tool

The aforementioned annotation tool was developed in a previous project for the purpose of trajectory reconstruction of lane-changing vehicles, using forward-roadway footage. The tool is based on manual annotation by the annotator: the annotator is requested to define the placement of different objects in the frame and the annotations are then used to calculate the relative distances between the defined objects and the SV. The annotator does not have to define the location of the objects for all frames, because the tool can interpolate the annotation between frames, to speed up the annotation process. This is described in more detail in El Din et al. [23]. The tool output is an object containing the relative speeds and distances to the POV and the lanes. Although the tool was mainly developed during the previous project, the first part of this thesis project was dedicated to improve its usability and add functions to the tool. Note that the forward-roadway footage used in this section is not taken from SHRP2 videos, as that would be in violation of the data licensing agreement. Instead, sample free to use video was used to showcase the functionality of the tool.

2.2.1.1 Video Player and Controls

Upon initialisation, the annotator is asked to choose an event to annotate from a list. The program will then take the ID number of said event and find the associated video and time-series data from the data-set stored in annotation rooms' computers at SAFER. Once loaded, the annotator is presented with the view shown in 2.4, where the frame number and event ID have been removed, in compliance with the data license agreement. Using the control buttons on the right, the annotator can annotate different elements for the selected frame. The different input options are explained in later sections.

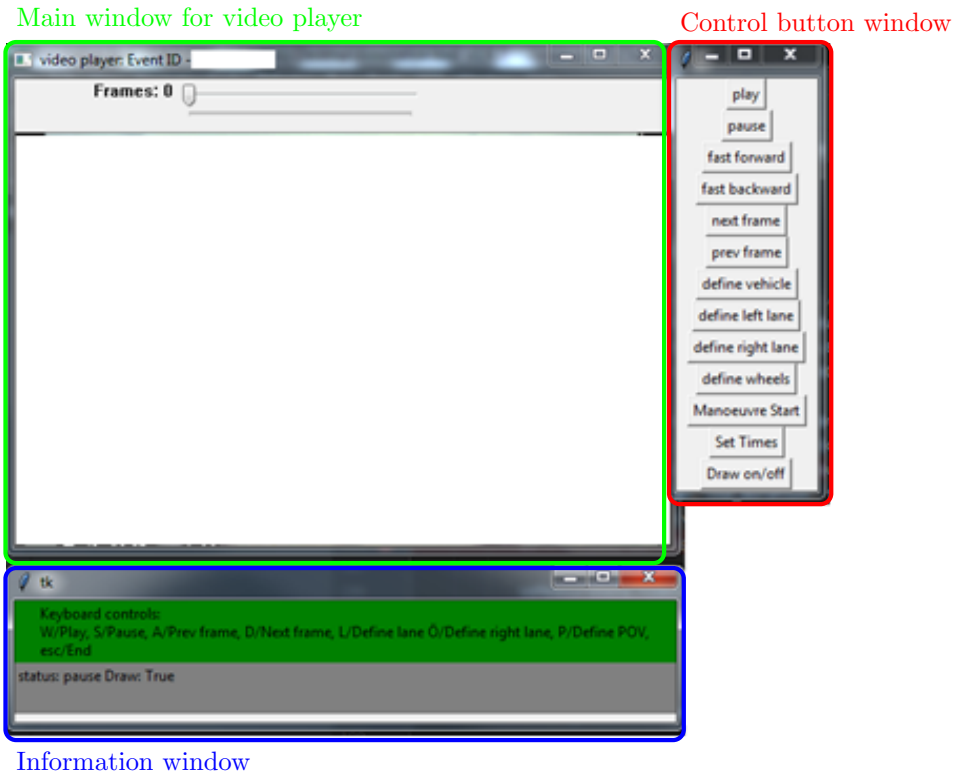

Figure 2.4: *Overview of GUI of the annotation tool*

2.2.1.2 Define POV Placement in the Frame

The POV placement is defined in the frame by drawing a bounding box around its rear width. This was defined as the distance between the outer most parts of the POV's tail lights. The corresponding image coordinates for the box are then used to calculate the lateral and longitudinal distances between the SV and the POV. Calculating distances using the POV width in an image has been researched in the past and was found to produce reasonable results [27]. Figure 2.5 shows the different stages of the annotation process for establishing the location of the POV. The annotator is asked to draw a box approximately around the rear of the POV, using the the mouse to click and drag (figure 2.5a). If the annotator is not satisfied with the annotation, they can redraw the box through using the mouse (figure 2.5b), then press the 'Enter' key to confirm the selection (figure 2.5c).

(a) *User pressed the button to define the POV* (b) *User is defining the POV (Blue), using the box*

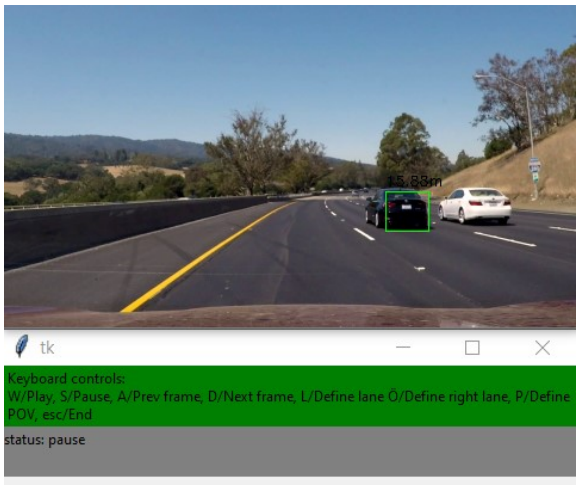

(c) *User has confirmed the input (Green)*

Figure 2.5: *The different stages of the annotation process to define the size of the POV*

As the annotator is annotating, the output ranges are constantly being plotted in two separate windows, against all radar targets that are available from the time-series data as seen in figure 2.6. This was done to help visualise the output to the annotator as they are annotating. If the output was unreasonable during some part of the event, the annotator would be able to navigate to that time in the event and improve the annotation.

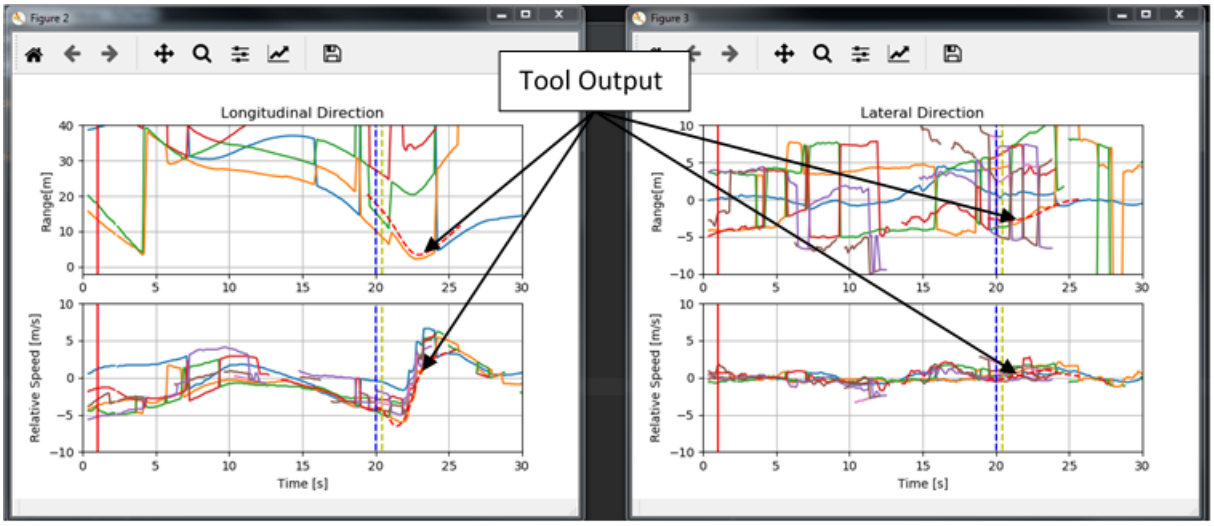

Figure 2.6: *Plots comparing the longitudinal range resulting from the tool and from the radar measurements (the tool output is the red dotted line and the radar measurements are all solid lines)*

Figure 2.6 serves also as motivation to why relying only on radar data for extracting the lateral and longitudinal ranges to the POV is challenging. The radar system used in the SHRP2 DAS could track 7 objects at the same time as seen in figure 2.6, where each solid coloured line represents one of the tracked targets, each with a specified target ID. This target ID could however change during the manoeuvre, meaning that the target ID for the POV would change during a manoeuvre. For instance, in figure 2.6, the POV is the red target ($t = 0 - 7[s]$), then green ($t = 7 - 16[s]$), then orange ($t = 16 - 18[s]$), then green ($t = 18 - 21[s]$), then orange ($t = 21 - 24[s]$) and finally blue ($t = 24 - 30[s]$). One would therefor need to manually identify which target ID is that of the POV at different times, which was challenging.

2.2.1.3 Defining lane lines and POV wheels

The lanes are defined through selecting points on the frame where the lanes are visible, using the mouse. When this is done, the slope of the line is calculated and the lanes are drawn on the frame, as see in red line (left lane) and aqua line (right lane) in figure 2.7. The wheels are defined in a similar fashion by selecting two points on the ground where the POV wheels touch the ground, as shown by the red circles in figure 2.7. The wheels were used to calculate the heading angle of the POV, relative to the lane. The heading was not part of the parameters used for the statistical modelling and was therefore not annotated for all events.

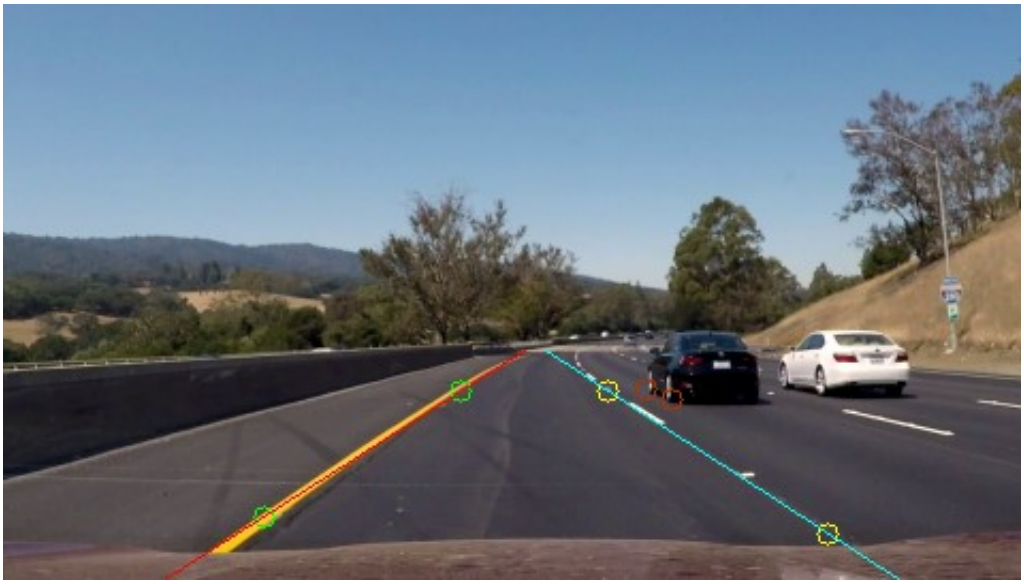

Figure 2.7: *User defined left lane line (green circle), right lane line (yellow circle) and POV wheels (red circle)*

2.2.1.4 Added Functionality To the Annotation Tool

During this project, the tool had to be further developed to improve usability and accuracy. The added functionalities are summarised in this section. A user manual that was written to explain the annotation process and controls is also included in appendix A.2.

Refining the POV Placement In the Frame

In the original tool, the only input option to define the bounding box around the rear of the POV was the mouse. As the tool was used more often at the beginning of this project, it was noticed that this method could take several attempts to get draw this box accurately. This was solved though assigning keyboard controls to move and enlarge/reduce the bounding box to refine the selection seen in figure 2.5b. This was found to speed up the annotation process and improve the stability of the tool output.

Removing Offset Between Tool Output and Radar Data

A known limitation of the original tool was that the output longitudinal range would often be offset from that of the longitudinal range measured by the radar, as seen in figure 2.8a. A quick solution was found to remove this offset by allowing the annotator to refine the output using the keyboard buttons: by pressing the '+' and '-' keys, the annotator would change the SV hood length. With this functionality, the annotator can remove any potential offset in the computed longitudinal range compared to the available radar range available from the time-series data, as seen in figure 2.8b. Changing the SV hood length was a quick solution to this problem, as the camera was mounted in the on the rear view mirror, while the radar was mounted next to the number plate closer to the target objects in-front.

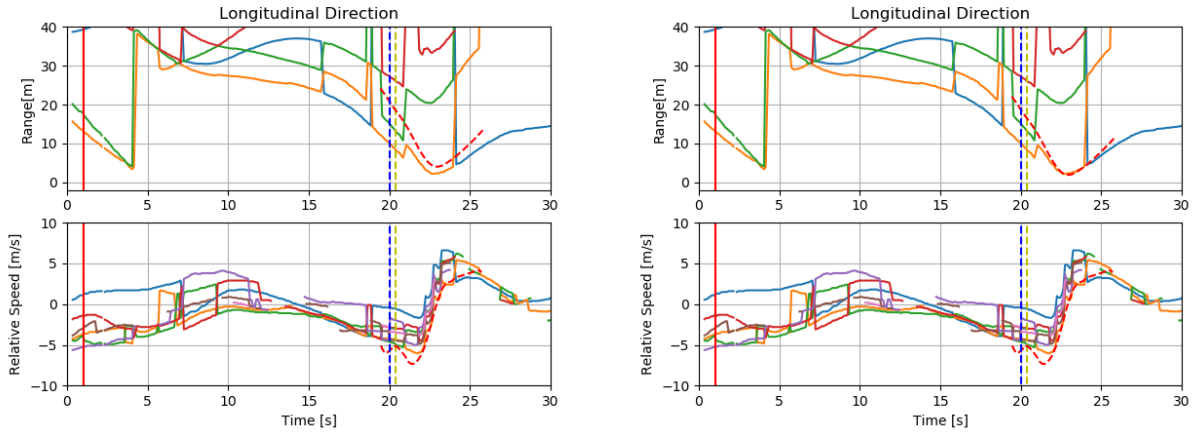

(a) *Longitudinal range before offset correction*

(b) *Longitudinal range after offset correction*

Figure 2.8: *Manual offset correction of longitudinal range (tool output is red dotted line and radar measurements are all solid lines)*

Defining Manoeuvre Start, POV Lane Cross and POV Blinker Start

The original tool did not have the option to annotate these parameters. These were added later as part of this project an potential future projects. The manoeuvre start is simply defined by the annotator as the frame number of the first frame where the annotator has defined all inputs described above. This information is only used later in the analyses, to know where the useful part of the output is located. The POV lane cross is the number of the frame where the annotator sees that any of the POV wheels has passed the left or right lines, to enter the target lane where the SV is travelling. The POV blinker start is the frame number where the annotator sees that the POV has started blinking. Both the POV Lane cross and the POV blinker start were considered as possible parameters for the statistical modelling.

Making a List with Relevant Events

In the original tool, the annotator was asked to pick a file location from the SAFER computer manually. This meant that for each annotation, the annotator would have to navigate to the folder containing these events to select one. As it was known that not all event would be suitable for annotation, a list containing all relevant events was developed. This would pop-up at the start of the annotation and allow the annotator to directly select an event, which was less time consuming. Moreover, as it became apparent that no part-time workers would be hired to do the annotation process, this list was divided in sub-folders for each of the five annotators that supported the annotation process, including the author. Under each sub folder were the events that were assigned to each annotator, which helped keep track the events that were annotated and allowed the annotator to specify a reason to exclude an event. This list in included in appendix A.1

2.3 Extraction of Manoeuvre kinematics

The raw output from the tool could not be used to describe the trajectories of the POV and SV. Instead, it had to be converted to a global axis to get the same representation for all events. After extracting the trajectories from the output, the lane-change manoeuvre itself was isolated for each event, based on predefined conditions described in this section. Last, the isolated lane-changes were parameterised using Ridge Regression in preparation for the statistical modelling.

2.3.1 Extracting trajectories for single events

After annotation is done, all distances in the tool output are relative to the SV (i.e. dash-cam). For easier comparison between events, all distances were converted to be referenced to the center of the target lane. The goal was to make a top-view map of the event. To do this, longitudinal and lateral distances had to be converted to global axes, as illustrated in figure 2.9. The parameters that were used, their notations and how they were obtained are tabulated in table 2.2. How these parameters were calculated is detailed later in this section.

Notation	Unit	Description	Source
$R_{Y,pov}$	m	Lateral range to POV	Available from tool output
$R_{X,pov}$	m	Longitudinal range to POV	Available from tool output
$Y_{LL,sv}$	m	Lateral distance from SV center to left lane	Available from tool output
$Y_{RL,sv}$	m	Lateral distance from SV center to right lane	Available from tool output
$Y_{LC,sv}$	m	SV lateral offset from lane center	Calculated using $Y_{LL,sv}$ and $Y_{RL,sv}$
$Y_{LC,pov}$	m	POV lateral offset from lane center	Calculated from $Y_{LC,sv}$ and $R_{Y,pov}$
$V_{X,sv}$	m/s	Longitudinal SV speed	Available from time-series data
$V_{Y,sv}$	m/s	Lateral SV speed in lane	Calculated using $\dot{Y}_{LC,sv}$
$S_{X,sv}$	m	Distance travelled by SV since start of event	Calculated using $\int V_{x,sv}$
$V_{X,pov}$	m/s	Longitudinal POV speed	Calculated using $\dot{S}_{X,pov}$
$V_{Y,pov}$	m/s	Lateral POV speed in lane	Calculated using $\dot{Y}_{LC,pov}$
$S_{X,pov}$	m	Distance travelled by POV since start of event	Calculated using $S_{X,sv}$ and $R_{X,pov}$

Table 2.2: Notations used for speeds and distances

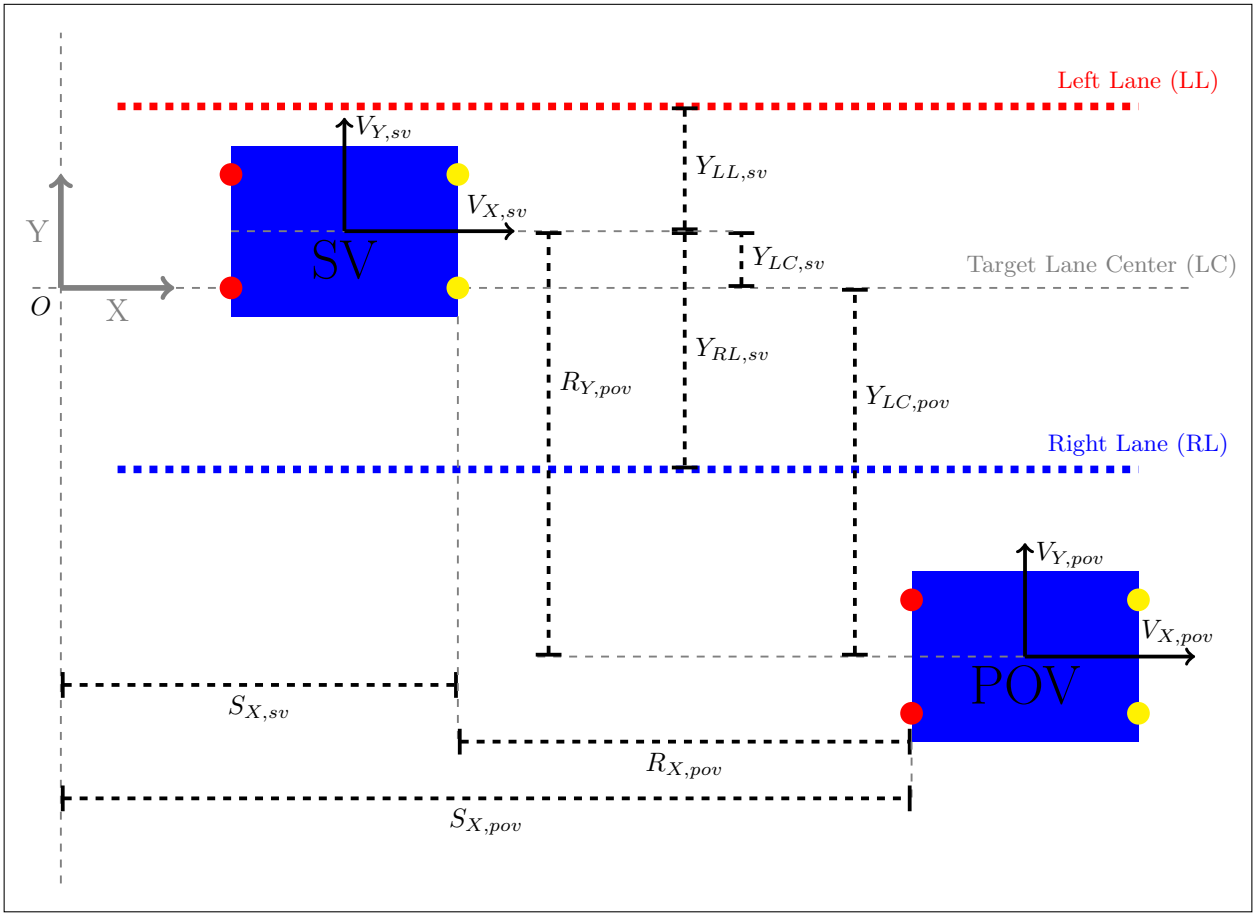

Figure 2.9: *Coordinate system with reference to target lane*

2.3.1.1 Longitudinal Distances $S_{X,sv}$ and $S_{X,pov}$

There was no data available about the distance that the SV had travelled. A solution was found, by estimating the distance travelled $S_{X,sv}$ through integrating the SV forward speed $V_{X,sv}$. Both GPS speed and CAN speed were available in the data. As the CAN speed was sampled at a higher rate and was overall more stable, it was chosen to calculate the travelled distance as by the SV:

$$S_{X,sv}(t) = \int_0^t V_{X,sv}(t)dt \tag{2.1}$$

The longitudinal distance travelled by the POV was then calculated as:

$$S_{X,pov}(t) = S_{X,sv}(t) + R_{X,pov}(t) \tag{2.2}$$

2.3.1.2 Lateral Offsets from lane center $Y_{LC,sv}$ and $Y_{LC,pov}$

Assuming that the target lane is straight and that the dash-cam is mounted at the center of the SV, the lane center Y_{LC} was defined as:

$$Y_{LC} = \frac{Y_{LL,sv} + Y_{RL,sv}}{2} \tag{2.3}$$

The SV lateral offset to the center of the lane was then defined as:

$$Y_{LC,sv} = 0 - Y_{LC} \tag{2.4}$$

This calculation was computed to reference the lateral distance in the lane to the lane center, as illustrated in figure 2.9. With the relative range $R_{Y,pov}$ to the POV known, the lateral distance from the target lane center to the POV was calculated as:

$$Y_{LC,pov} = R_{Y,pov} - Y_{LC,sv} \tag{2.5}$$

2.3.1.3 Speeds $V_{Y,sv}$, $V_{Y,pov}$ and $V_{X,pov}$

The lateral speeds were defined as the rate of change in the lateral distance from the lane center for both the SV and the POV. This was done through simple differentiation of $Y_{LC,sv}$ and $Y_{LC,pov}$ respectively as:

$$V_{Y,sv} = \dot{Y}_{LC,sv} \tag{2.6}$$

$$V_{Y,pov} = \dot{Y}_{LC,pov} \tag{2.7}$$

The longitudinal POV speed $V_{X,pov}$ was calculated using the speed of the distance travelled by the POV $S_{X,pov}$ as:

$$V_{X,pov} = \dot{S}_{X,pov} \tag{2.8}$$

2.3.2 Define Start and End of lane change

After converting the raw output from to tool to the global coordinate system defined in 2.9, it was possible to distinguish different types of lane change manoeuvres using the POV position relative to the lane center. Through the initial annotation of 10 events, the following types of lane changes were observed:

- Single lane change
  - Lane change where the POV was in the adjacent lane at the start of the manoeuvre and it is in the target lane at the end of the manoeuvre, as illustrated in 2.10 (green)
- Double lane change at start of manoeuvre (double lane change start)
  - Lane change where the POV was outside the adjacent lane at the start of the manoeuvre; meaning that the POV is in the lane next to the adjacent lane; and it is in the target lane at the end of the maouver, as illustrated in figure 2.10 (red).
- Double lane change at end of manoeuvre (double lane change end)
  - Lane change where the POV was in the adjacent lane at the start of the manoeuvre and is outside the target lane at the end of the manoeuvre, as illustrated in figure 2.10 (blue).

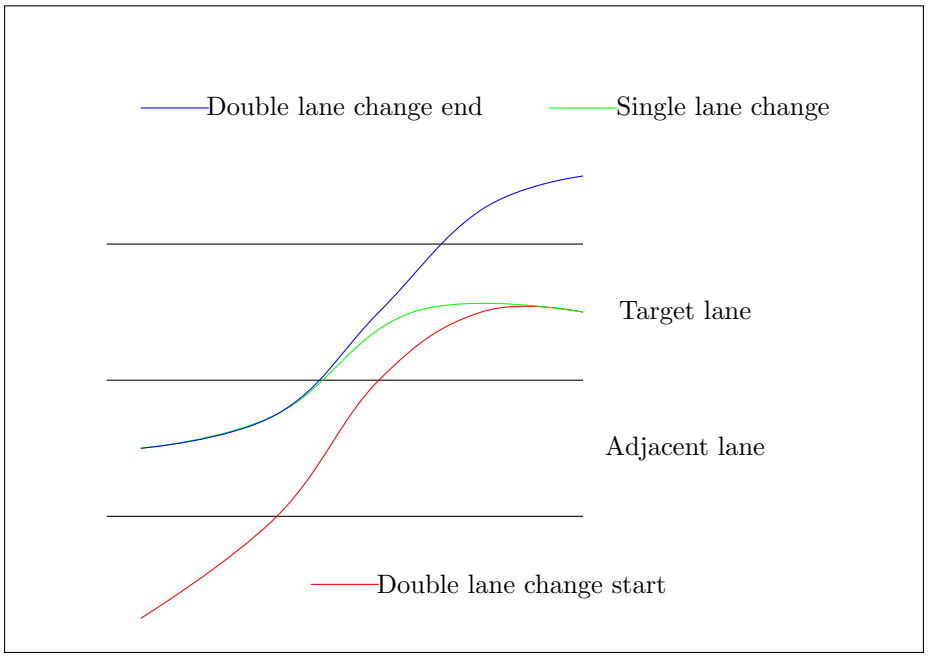

Figure 2.10: *Illustration of POV trajectory for the different type of lane-changes*

An algorithm was developed to find the start and end times for each of the manoeuvres using the POV lateral distances to the lane center $Y_{LC,sv}$ and the lateral speed $V_{X,pov}$, as described below.

The first step to identify if the POV is to the right or left adjacent lane, with respect to the SV. This was defined though using the first value in the lateral distance $Y_{LC,pov}$, as defined in 2.9 and 2.10. If the POV is in the left adjacent lane, then it is about to commence a lane change by moving to the right and vice versa.

$$Y_{LC,pov}(1) > 0 \Rightarrow \ \textit{POV is in the left adjacent lane} \tag{2.9}$$

$$Y_{LC,pov}(1) < 0 \Rightarrow \ \textit{POV is in the right adjacent lane} \tag{2.10}$$

The calculations used to determine the start and end times of different lane-change manoeuvres are explained below.

2.3.2.1 Single lane change

A manoeuvre is defined as a single lane change if the start position of the POV is less than 1.5 lane width away at the start of the manoeuvre; as this was assumed to be the outer edge of the adjacent lane; and is within the target lane by the end of the manoeuvre, as shown in 2.11. The lane width was calculated as the absolute distance between $Y_{LL,sv}$ and $Y_{RL,sv}$.

$$\begin{aligned} |Y_{LC,pov}(1)| < 1.5 * (|Y_{LL,sv}(1)| + |Y_{RL,sv}(1)|) \\ and, \Rightarrow single\ lane\ change \\ RL(end) < Y_{LC,pov}(end) < LL(end) \end{aligned} \tag{2.11}$$

The start of the manoeuvre $t_{pov,start}$ is defined as the time when the POV initiates the move towards the left (left lane change) or right (right lane change), in the direction of the target lane. In an ideal case, this would be identified as the local peak in the lateral distance $Y_{LC,pov}$, in a similar manner as was done by Wang, Yang, and Hurwitz [22]. The local maximum of $Y_{LC,pov}$ is by definition the point in time where the lateral speed $V_{Y,pov} = 0[m/s]$. However, since the output is obtained through manual annotation, $V_{Y,pov}$ was often noisy. Therefore, the start of the manoeuvre was identified using a threshold of $V_{Y,pov} = 0 \pm V_{Y,pov,trigger}$ rather than $V_{Y,pov} = 0$, where the trigger value $V_{Y,pov,trigger}$ is close to 0. A trigger value of $V_{Y,pov,trigger} = \pm 0.2[m/s]$ was found reasonable to identify the start of a manoeuvre. The sign of $V_{Y,pov,trigger}$ depended on the direction towards which the POV is commencing a lane-change, either to the right (right lane-change) or to the left (left lane-change), as shown in 2.12 and 2.13.

$$t_{pov,start} = t|_{(V_{Y,pov}=-0.2[m/s])},\ Right\ lane\ change \tag{2.12}$$

$$t_{pov,start} = t|_{(V_{Y,pov}=0.2[m/s])},\ Left\ lane\ change \tag{2.13}$$

It was found that this definition alone was not sufficient for most cases, since the lateral speed $V_{Y,pov}$ could be within the trigger threshold multiple times during an event. To find the correct start time, the peak of the lateral speed was used as either $min(V_{Y,pov})$ for right lane change or $max(V_{Y,pov})$ for left lane change. The start time $t_{pov,start}$ was then defined as the first time where the lateral speed crossed the threshold before $t_{pov,peak}$. The end time $t_{pov,end}$ was then defined as the first time where the lateral speed crosses the threshold after $t_{pov,peak}$. Both of these are illustrated in figure 2.11 for right lane change. The inverse is true for left lane change. Such events were labelled *'single lane change start'* and *'single lane change end'*.

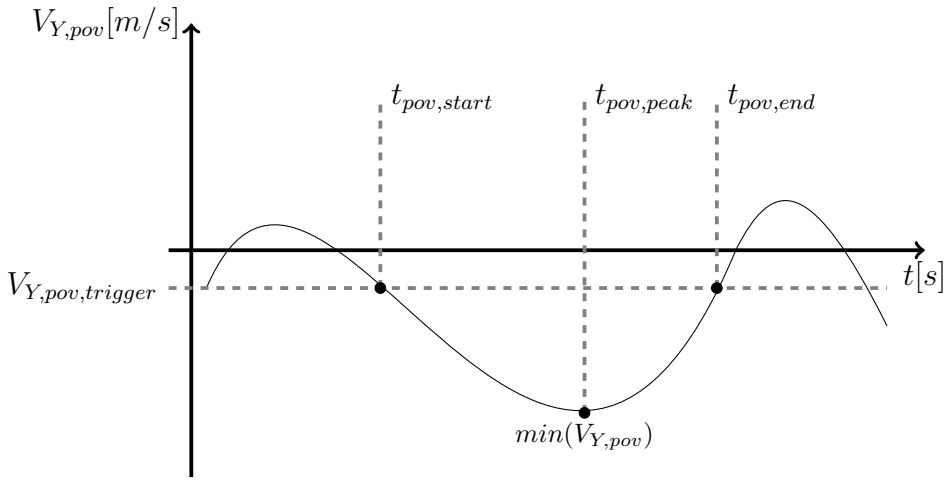

Figure 2.11: *Illustration of how the start and end of a manoeuvre is found for right lane change*

For some events, the lateral speed $V_{y,pov}$ did not have a clear peak. This was a result of the POV being too far away during the start of the manoeuvre to track accurately, since it appeared smaller in the image frame. For these cases, the start and end of the manoeuvre were defined the maximum and minimum values of $Y_{LC,pov}$ as shown in 2.14. These events were labelled *'hidden start'* and *'hidden end'*. This indicated that the POV was outside the adjacent lane.

$$\begin{aligned} t_{pov,start} &= max(Y_{LC,pov}) \text{ and } t_{pov,end} = min(Y_{LV,pov}), \text{ right lane change} \\ t_{pov,start} &= min(Y_{LC,pov}) \text{ and } t_{pov,end} = max(Y_{LV,pov}), \text{ left lane change} \end{aligned} \tag{2.14}$$

2.3.2.2 Double lane change start

An event is identified as a double lane change start if the first annotated value of the lateral distance $Y_{LC,pov}$ is more that 1.5 lane width away from the target lane center, as shown in 2.15.

$$|Y_{LC,pov}| > 1.5 * (|Y_{RL,sv}| + |Y_{LC,sv}|) \Rightarrow \text{double lane change start} \tag{2.15}$$

The start time of the lane change manoeuvre was then defined as the time where the POV crosses the center of the adjacent lane. Assuming that both lanes are of equal width, this was identified as the time where the POV is one lane width away from the lane centred, as shown in 2.16 where $LW = |Y_{RL,sv}| + |Y_{LC,sv}|$

$$t_{pov,start} = t|_{|Y_{LC,pov}|=LW} \tag{2.16}$$

The end time of the lane change was defined in the same manner as for a single lane change, as described in the previous section.

2.3.2.3 Double lane change end

An event is identified as a double lane change end if the last annotated value of the $Y_{LC,pov}$ is outside of the target lane as shown in 2.17 and 2.18.

$$Y_{LC,pov}(end) > LL(end), \text{ right lane change} \tag{2.17}$$

$$Y_{LC,pov}(end) < RL(end), \text{ left lane change} \tag{2.18}$$

The end of the manoeuvre was defined as the time where the POV crossed the center of the target lane. In these cases, the start time of the manoeuvre is defined in the same manner as for a single lane change as described in the previous section.

2.3.2.4 Scenario Duration

After defining the start and end time of each event, the scenario duration was then calculated as:

$$t_{pov,scenario} = t_{pov,end} - t_{pov,start}$$

2.3.3 Parameterising the Trajectory for single events

In preparation for the statistical modelling of the lane change manoeuvre, the extracted trajectories were parameterised. The goal was to fit a $5th$ degree polynomial to the lateral and longitudinal trajectories. Ridge Regression was suitable for this type of parameterisation as it has been used in previous research to estimate the turning trajectory of vehicles in intersections [28].

2.3.3.1 Linear Regression Analysis

Regression Analysis is a technique used to develop mathematical models to describe or explain the relationships between variables. The goal is to understand how a variable, called the dependant (or predicted or response) variable, is dependant on a set of independent (or regressor or explanatory) variables [29]. Regression using one single independent variable is known as uni-variant regression analysis, while Regression using one dependant variable and several independent variables is known as multi-variate regression analysis [30]. In such analysis, an attempt is made to account for the variation of the independent variables in the dependant one. For each observation i, this type of analysis is formulated as:

$$y_i = \beta_{i,0} + \beta_{i,1} \cdot x_{i,1} + ... + \beta_{i,n} \cdot x_{i,n} + \varepsilon_i$$

Where, y is the dependant variable, n is the number of independent variables, x_n are the independent variables, β_n are the model parameters and ε is an error.

This can also be rewritten as:

$$\mathbb{Y} = \mathbb{X}\boldsymbol{\beta} + \boldsymbol{\varepsilon}$$

Where, $\mathbb{Y}$ is an $(i \times 1)$ vector of observations, $\mathbb{X}$ is an $(i \times n)$ matrix with n predictors for each observation i, $\boldsymbol{\beta}$ is an $n \times 1$ vector of population values of the model parameters and $\boldsymbol{\varepsilon}$ is an $(i \times 1)$ vector of experimental errors [31]. The conventional estimator of $\boldsymbol{\beta}$ is the least squares estimator, $\hat{\boldsymbol{\beta}}$, where $\hat{\boldsymbol{\beta}}$ is chosen to minimise the sum of square residuals as:

$$\hat{\boldsymbol{\beta}} = (\mathbb{X}^T\mathbb{X})^{-1}\mathbb{X}^T\mathbb{Y}$$

The least square estimate is good if $\mathbb{X}^T\mathbb{X}$ is nearly a unit matrix. However, when $\mathbb{X}^T\mathbb{X}$ is not nearly a unit matrix, the last square estimates are sensitive to several errors, so that they do not hold meaningful value when put into the context of physical properties [32]. Ridge Regression, which is based on the standard model for linear regression using least square estimates, is one method to address the instability associated with the least square estimate [33]. This is done by introducing a ridge parameter k , as:

$$\hat{\boldsymbol{\beta}} = (\mathbb{X}^T\mathbb{X} + kI)^{-1}\mathbb{X}^T\mathbb{Y}$$

Where I is an identity matrix and $0 \leq k \leq 1$. Generally, there is an optimum value for k for any problem, but it is preferred to examine the ridge solution for a range of values for k [32].

This was implemented in MatLab using the $fitlinear()$ function for the lateral trajectory using $Y_{LC,pov}$ and $V_{Y,pov}$ and for the longitudinal trajectory using $S_{X,pov}$ and $V_{X,pov}$, as described in the sections below.

Lateral Trajectory

Since $Y_{LC,pov}$ and $V_{Y,pov}$ had a physical relation where $V_{Y,pov} = \frac{d}{dt}Y_{LC,pov}$, they were both input as observations to the regression model, to improve the parameter estimation. Since the goal was to estimate the trajectory over time, different powers of the event time $t^{(0:5)}$ were used as predictors where:

$$t^{(0:5)} = \begin{bmatrix} t^0 & t^1 & . & . & . & t^5 \end{bmatrix}$$

The observation matrix $\mathbb{Y}_{lat}$ and predictor matrix $\mathbb{X}_{lat}$ were then defined as:

$$\mathbb{Y}_{lat} = \begin{bmatrix} {Y_{LC,pov}}_{(i\times 1)} \\ {V_{Y,pov}}_{(i\times 1)} \end{bmatrix}_{(2i\times 1)}, \mathbb{X}_{lat} = \begin{bmatrix} {t^{(0:5)}}_{(i\times 6)} \\ \frac{d}{dt}({t^{(0:5)}})_{(i\times 6)} \end{bmatrix}_{(2i\times 6)} \tag{2.19}$$

Where i is the number of annotated frames (data-points) and 6 is the number of predictors. Finally, the model parameters $\hat{\boldsymbol{\beta}}_{lat}$ were estimated as:

$$\hat{\boldsymbol{\beta}}_{lat} = \left[(\mathbb{X}_{lat}{}^{T}\mathbb{X}_{lat} + kI)^{-1}\mathbb{X}_{lat}{}^{T}\mathbb{Y}_{lat}\right]_{(6\times1)}$$

Where the ridge parameter $k = 10^{-4}$ was chosen as it provided good predictions. The estimated lateral trajectory $\hat{\mathbb{Y}}_{lat}$ was then calculated as:

$$\hat{\mathbb{Y}}_{lat} = \left[\mathbb{X}_{lat}\,\hat{\boldsymbol{\beta}}_{lat}\right]_{(2i\times1)}$$

Where:

$$\hat{Y}_{LC,pov} = \hat{\mathbb{Y}}_{lat}(1:i) \;\; and, \; \hat{V}_{Y,pov} = \hat{\mathbb{Y}}_{lat}(i+1:end)$$

Longitudinal Trajectory

$S_{X,pov}$ and $V_{X,pov}$ were parameterised similarly to the formulation described above for the lateral trajectory where the observation matrix $\mathbb{Y}_{long}$ and the predictor matrix $\mathbb{X}_{long}$ were defined as:

$$\mathbb{Y}_{lat} = \begin{bmatrix} S_{X,pov}{}_{(i\times1)} \\ V_{X,pov}{}_{(i\times1)} \end{bmatrix}_{(2i\times1)}, \; \mathbb{X}_{long} = \begin{bmatrix} t^{(0:5)}{}_{(i\times6)} \\ \frac{d}{dt}(t^{(0:5)})_{(i\times6)} \end{bmatrix}_{(2i\times6)} \tag{2.20}$$

The model parameters $\hat{\boldsymbol{\beta}}_{long}$ were estimated as:

$$\hat{\boldsymbol{\beta}}_{long} = \left[(\mathbb{X}_{long}{}^{T}\mathbb{X}_{long} + kI)^{-1}\mathbb{X}_{long}{}^{T}\mathbb{Y}_{long}\right]_{(6\times1)}$$

Where the ridge parameter was kept the same as for the lateral range estimation ($k = 10^{-4}$). The estimated longitudinal trajectory $\hat{\mathbb{Y}}_{long}$ was then calculated as:

$$\hat{\mathbb{Y}}_{long} = \left[\mathbb{X}_{long}\,\hat{\boldsymbol{\beta}}_{long}\right]_{(2i\times1)}$$

Where:

$$\hat{S}_{X,pov} = \hat{\mathbb{Y}}_{long}(1:i) \;\; and, \; \hat{V}_{X,pov} = \hat{\mathbb{Y}}_{long}(i+1:end)$$

The model parameters $\hat{\boldsymbol{\beta}}_{lat}$ and $\hat{\boldsymbol{\beta}}_{long}$ were indented to be used for the statistical modelling of the lane change. However, few of the annotated events had captured the entire lane-change manoeuvre. This, alongside the limited accessibly to the SAFER due to the Covid-19 pandemic, resulted in redirecting the aim of the thesis to modelling the uncertainty of the annotated variables instead.

2.4 Uncertainty modelling

The annotations were performed by five persons in this project. It was therefore important to investigate how the output of the annotations varied for different users. A total of 10 events were chosen and annotated by all five users. The outputs these events were then studied to estimate the uncertainty of the results. This was done for the following variables, directly extracted from the tool: $R_{Y,pov}$, $R_{X,pov}$, $Y_{LL,sv}$, $Y_{RL,sv}$.

2.4.1 Uncertainty of $R_{X,pov}$ and $R_{Y,pov}$

As initially anticipated, the output ranges were not equal for all annotators. In this section, $R_{X,pov}$ and $R_{Y,pov}$ will be refereed to as R_X and R_Y, to simplify the expressions. To estimate the error for each event, the averages $R_{X,av}$ and $R_{Y,av}$ of all five annotators were calculated as:

$$R_{X,av} = \frac{\sum_{u=1}^{5} R_{X,u}}{5}, \quad R_{Y,av} = \frac{\sum_{u=1}^{5} R_{Y,u}}{5}$$

Where $u = (1:5)$ is each of the five annotators. The errors $R_{X,u,err}$ and $R_{Y,u,err}$ for each annotator were then calculated through subtracting the average from their output as:

$$R_{X,u,err} = R_{X,u} - R_{X,av}, \quad R_{Y,u,err} = R_{Y,u} - R_{Y,av}$$

Initially, it was thought that the errors $R_{X,u,err}$ and $R_{Y,u,err}$ were only dependent on R_X. This is due to that fact that a larger R_X meant that the POV was further away and thus appeared smaller in the image frame. When the POV was smaller in the frame, it was difficult to define the bounding box around the rear width of the vehicle. This was known from the previous project in which this tool was developed [23]. However, after analysing the calculated errors, it was clear that R_Y also affected $R_{X,u,err}$ and $R_{Y,u,err}$ at closer R_X ranges. This meant that the uncertainty of the output was best estimated as a function of both R_X and R_Y. The standard deviation of $R_{X,u,err}$ and $R_{Y,u,err}$ were used as a metric to model the uncertainty.

The standard deviation is used to measure variance in a data-set. For a normally distributed data-set, around 95% of all values will be within 2 standard deviations of the mean of all values giving a 95% confidence interval [34]. The other 5% should be equally scattered above and below these limits. The outputs from only 9 events (events (2-9)) were used for the uncertainty models, with the remaining event (event 1) spared to test the developed models. The goal was to use linear regression to estimate the standard deviations of $R_{X,u,err}$ and $R_{Y,u,err}$ as functions of $R_{X,av}$ and $R_{Y,av}$.

2.4.1.1 Uncertainty of R_X

For each data-point, the standard deviation of all five errors was calculated. These were then used as observations in the regression model. To achieve this, the errors of all five users were combined into one matrix where each column contained $R_{X,u,err}$ of one annotator for the all 9 events (2-10) that were chosen to train the model as:

$$E_X = \begin{bmatrix} R_{X,1,err,2} & R_{X,2,err,2} & .. & R_{X,5,err,2} \\ R_{X,1,err,3} & R_{X,2,err,3} & .. & R_{X,5,err,3} \\ : & : & .. & : \\ : & : & .. & : \\ R_{X,1,err,10} & R_{X,2,err,10} & .. & R_{X,5,err,10} \end{bmatrix}_{(4050\times5)} \tag{2.21}$$

Where E_X is the longitudinal error matrix. Since each event contains 450 frames, this matrix had $450 * 9 = 4050$ rows. The standard deviation SD_X of each row was then calculated using the *std()* function in MATLAB as:

$$SD_X = \left[std(E_X)\right]_{4050\times1} \tag{2.22}$$

The average ranges $R_{X,av}$ and $R_{Y,av}$ for all 10 events were combined into two vectors; P_X and P_Y; to be used as predictors:

$$P_X = \begin{bmatrix} R_{X,av,2} \\ R_{X,av,3} \\ : \\ R_{X,av,10} \end{bmatrix}_{4050\times1} \quad , \quad P_Y = \begin{bmatrix} R_{Y,av,2} \\ R_{Y,av,3} \\ : \\ R_{Y,av,10} \end{bmatrix}_{4050\times1} \tag{2.23}$$

Regression was then done in MATLAB using the *regress()* function as:

$$a_X = \left[regress(SD_X, [P_X P_Y])\right]_{2\times1} \tag{2.24}$$

Where the output a_X was a matrix with one column and two rows. Each row contained one coefficient for each predictor. The standard deviation of the error could then be estimated for any data-point i of the longitudinal range $R_{X,i}$ and the lateral range $R_{Y,i}$ using these coefficients as:

$$\hat{SD}_{X,i} = \left(\begin{bmatrix} R_{X,i} & R_{Y,i} \end{bmatrix} a_X\right)_{(1\times1)} \tag{2.25}$$

Where $\hat{SD}_{X,i}$ is the estimated standard deviation of the error. For simplicity, the error was assumed to be normally distributed. This allowed to model the uncertainty with a 95% confidence interval using $2 * \hat{SD}_{X,i}$. This means that for each data-point, 95% of the errors should be within $2 * \hat{SD}_{X,i}$. The uncertainty of the longitudinal the error $\hat{R}_{X,u}$ for each annotation could then be estimated as:

$$\hat{R}_{X,u} = R_{X,u} \pm 2 * \begin{bmatrix} R_{X,u} & R_{Y,u} \end{bmatrix} a_X \tag{2.26}$$

Uncertainty of R_Y

The uncertainty of R_Y was estimated using the same method as for R_X. The combined lateral error matrix E_Y was defined as:

$$E_Y = \begin{bmatrix} R_{Y,1,err,2} & R_{Y,2,err,2} & .. & R_{Y,5,err,2} \\ R_{Y,1,err,3} & R_{Y,2,err,3} & .. & R_{Y,5,err,3} \\ : & : & .. & : \\ : & : & .. & : \\ R_{Y,1,err,10} & R_{Y,2,err,10} & .. & R_{Y,5,err,10} \end{bmatrix}_{(4050\times5)} \tag{2.27}$$

The standard deviation SD_Y of each row was then calculated using the *std()* function in MATLAB as:

$$SD_Y = \left[std(E_Y)\right]_{4050\times1} \tag{2.28}$$

The predictors P_X and P_Y were kept the same as 2.23. Regression was then done using the *regress()* function in MATLAB as:

$$a_Y = \left[regress(SD_Y, [P_X P_Y])\right]_{2\times1} \tag{2.29}$$

Finally, the uncertainty of the lateral range $\hat{R}_{Y,u}$ for each annotation could be calculated as:

$$\hat{R}_{Y,u} = R_{Y,u} \pm \begin{bmatrix} R_{X,u} & R_{Y,u} \end{bmatrix} a_Y \tag{2.30}$$

2.4.2 Uncertainty of $Y_{LL,sv}$ and $Y_{LC,sv}$

From the SVs' perspective, the lanes were assumed to be two parallel line that stretched along the length of the road way. This meant that the lanes lines have no longitudinal range component that can be used to model the uncertainty. Instead, the uncertainty would be estimated using the standard deviation of the error across annotators. In this section, $Y_{LL,sv}$ and $Y_{LC,sv}$ will be referred to as Y_{LL} and Y_{LC} to simplify the expressions. To estimate the error for each event, the averages $Y_{LL,avg}$ and $Y_{LC,avg}$ of all five annotators were calculated as:

$$Y_{LL,av} = \frac{\sum_{u=1}^{5} Y_{LL,u}}{5}, \quad Y_{LR,av} = \frac{\sum_{u=1}^{5} Y_{RL,u}}{5}$$

Where $u = (1:5)$ is for each of the 5 annotators. The errors $Y_{LL,u,err}$ and $Y_{RL,u,err}$ for each annotator were then calculated as:

$$Y_{LL,u,err} = R_{X,u} - R_{X,av}, \quad Y_{RL,u,err} = R_{Y,u} - R_{Y,av}$$

The uncertainty of the lane-lines were then evaluated through studying the mean and standard deviations of the errors for all 10 events. If $Y_{LL,u,err}$ and $Y_{RL,u,err}$ have large mean and standard deviation values, this would mean that the uncertainty of Y_{LL} and Y_{LC} is large. If $Y_{LL,u,err}$ and $Y_{RL,u,err}$ have low mean and standard deviation values, this would mean that the uncertainty of Y_{LL} and Y_{LC} is low.

3 Results

The results of data pre-pocessing, annotation of data, extraction of manoeuvre kinematics and uncertainty modelling are presented in this section.

3.1 Pre-processing and Annotation of Data

3.1.1 Converting data format and Re-structuring data

The effects of the synchronisation issue that was described in section 2.1.1 are best visualised by comparing the range to the POV from both the tool output and the radar data. This was done for event 1 where the effect was visible, as shown in figure 3.1. In this figure, the longitudinal range to the POV reaches its minimum value of $\approx 15[m]$. Before correction, the tool output (red dotted line) reaches this value at $\approx 24[s]$ while the radar range reaches $\approx 15[m]$ at $\approx 23[s]$. This is due to the video footage starting $\approx 1[s]$ before the time series data. After correction, both the radar range and to tool output range reach the minimum value of $\approx 15[m]$ at $\approx 24[s]$. It was important to have the time-series data synchronised with the radar range since the distance travelled by the SV ($S_{X,sv}$) is calculated through integration of the CAN speed available from the time-series data, as explained in section 2.3.1.3. Having an offset between the time-series data and the tool output would therefore result in an inaccurate $S_{X,sv}$ estimation.

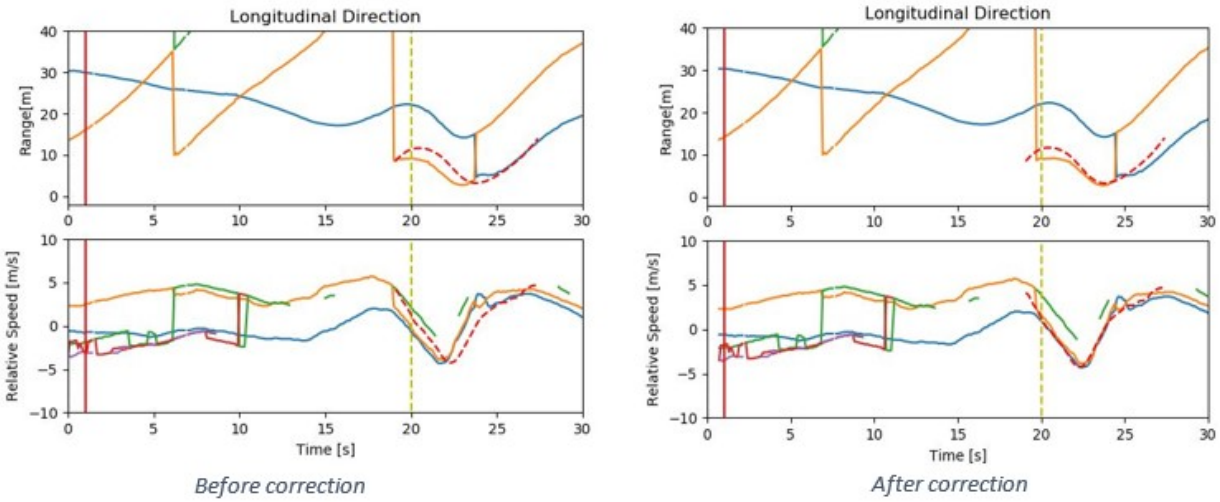

Figure 3.1: *Effect of synchronisation issue (event 1) (Red-dotted line is tool output and yellow radar target betwee $t = 20 - 24[s]$ is POV)*

3.1.2 Identification of Relevant Events and Annotation

Out of the 1191 events, 241 fit the criteria mentioned in 2.1.2. These events were then screened manually by the author, using the tool, to determine if they are suitable for annotation. Based on the screening, 86 events were chosen for the annotation process. The other 169 events were excluded from the analysis based on the motivations tabulated in table 3.1.

The frequency of these motivations are shown in figure 3.2. The most common motivation was that the POV did not do a complete lane change. Other common motivations were: POV is a truck, POV is out of frame, missing radar data and SV changes lane

After it became clear that no part-time annotators would be hired, it was decided to split 60 of the 86 suitable events among the three project supervisors, one project assistant and the author. Each of the three

supervisors and one project assistant would annotate 10 events, while the author would annotate 20. An additional 10 events were annotated by all five annotators to make a total of 70 events. Due to the bounded time frame of the project and the limitations brought by the covid-19 outbreak, only 57 of the 70 events were annotated, 10 of which were annotated by all five annotators. All involved annotators have undergone a course on how to treat personal data, as required by VTTI.

Motivation	Description
POV does partial (incomplete) lane-change	As the initial aim was to model completed lane-changes, partial lane changes were not considered for annotation.
The POV is not a passenger vehicle	In many cases the POV were trucks. These could not be annotated since trucks were too big and were partially outside the frame during the manoeuvre.
POV out of frame	In these cases, the POV would be outside the image frame during some part of the manoeuvre. It was therefore not possible to track the POV.
Missing radar data or SV can speed	The radar measurements and SV CAN speed available in the time-series were sometimes incomplete or missing.
SV changes lane	In these cases, the SV would also be doing a lane-change manoeuvre at the same time as the POV. Tracking the left and right lane lines was then not accurate, as the SV would be moving laterally from one lane to other. These events were also excluded as the initial scope of the project was to model completed lane-changes where the SV stayed in the same lane during the entire manoeuvre.
Lanes are too wide	In these cases, two lanes would be merging together at the start of the manoeuvre. As a result, the left and right lane lines would be too far apart.
POV is obscured	In these cases, the POV would be obscured by other vehicles during the start of the lane-change manoeuvre. It was therefore not possible to track the POV.
POV is too far away	Cases where the POV was too far away ($> 40[m]$) during the beginning of the manoeuvre to track accurately as the POV would be small in the image frame.

Table 3.1: Description of the excluded events after manual screening of 241 events

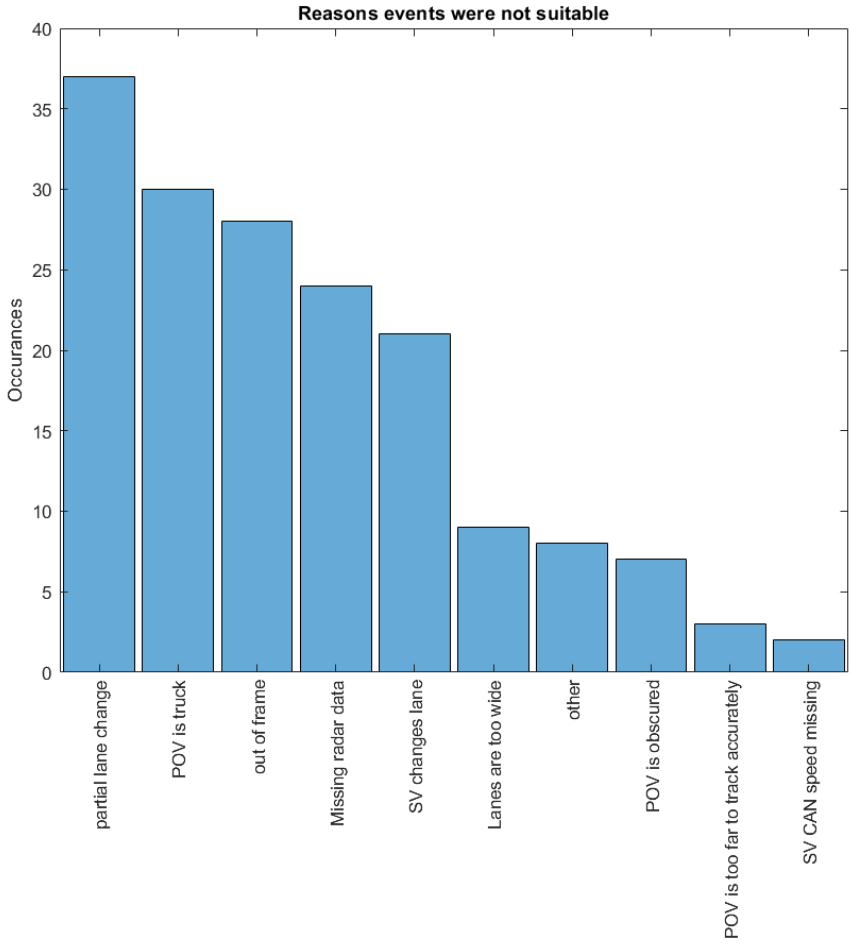

Figure 3.2: *Number of events discarded and corresponding motivations, based on the screening of events*

The TTC of the 57 annotated events were calculated. These are shown in figure 3.3 alongside the mean and standard deviation. For comparison, Lee, Olsen, Wierwille, et al. [17] had found that 95% of drivers feel comfortable during a lane-change when the TTC was above $4[s]$. This suggests that most of the annotated events are indeed critical.

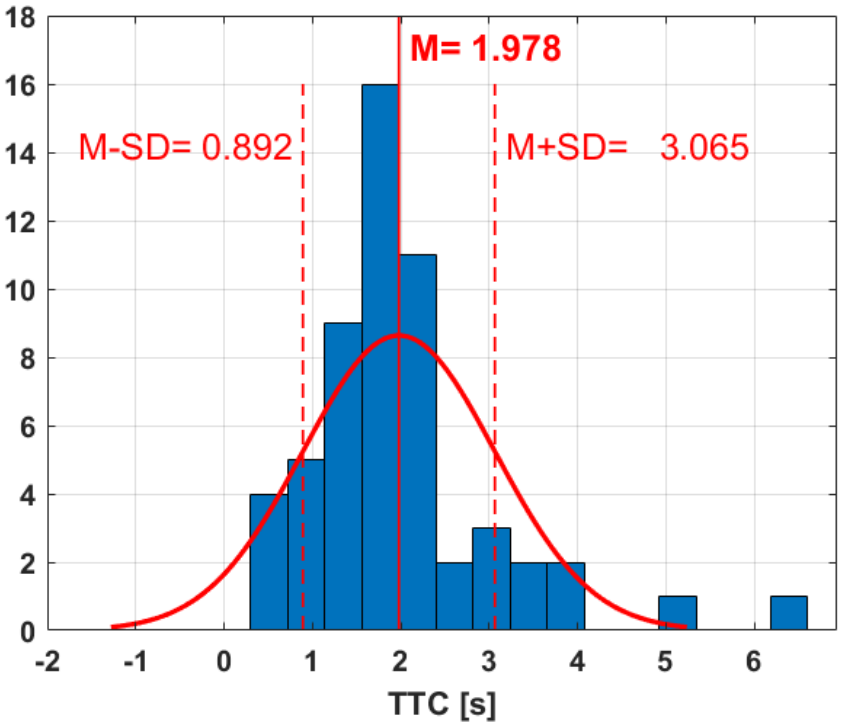

Figure 3.3: *TTC of the 57 annotated events*

3.2 Extraction of Manoeuvre kinematics

In preparation for the statistical modelling of lane-change manoeuvres, the functions needed to extract the manoeuvre kinematics were completed. They are therefore included here as valuable input for future projects within this subject.

3.2.1 Extracting trajectory for single events

The goal was to combine the tool output; $R_{X,pov}$ and $R_{Y,pov}$ plotted in figure 3.4; with the time-series data and be able to make a top-view map of each event, as illustrated in figure 3.5. This was done as described in the methodology. In this section, the calculations are presented for extracting the trajectory of event 1, starting from the raw tool output. The same procedure could be applied to the other events.

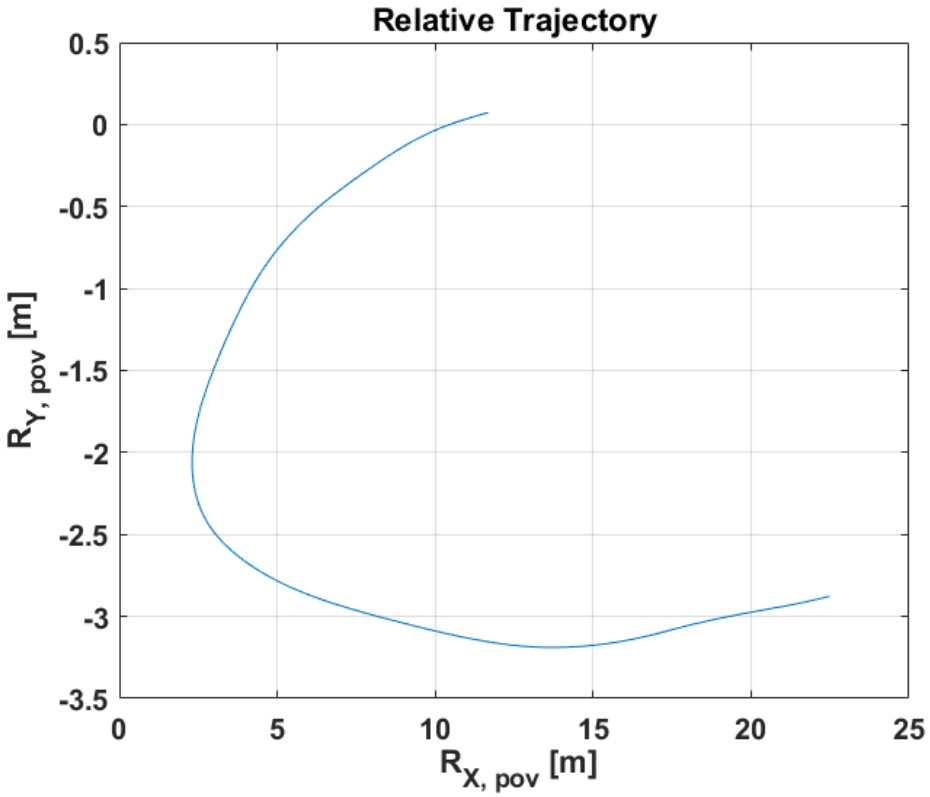

Figure 3.4: *The relative trajectory available form the tool output (event 1)*

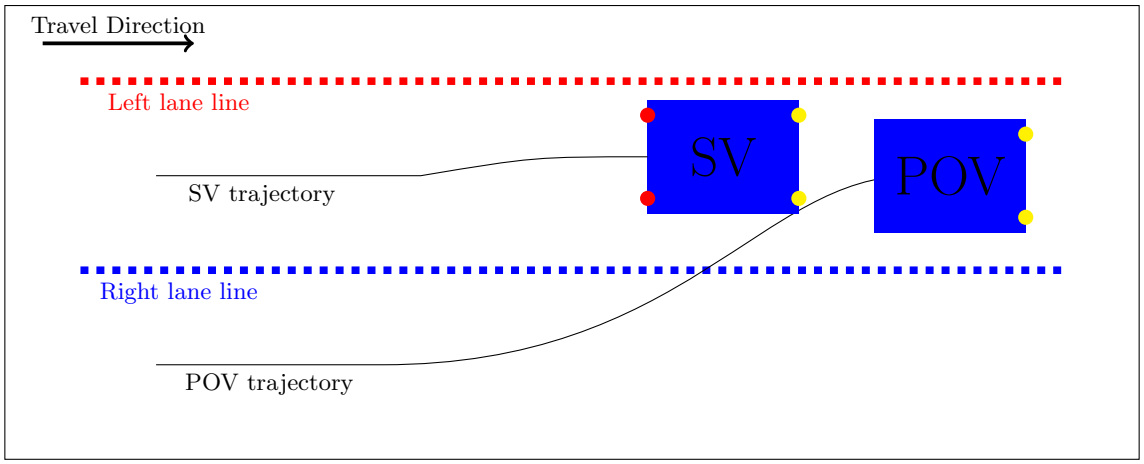

Figure 3.5: *Goal of trajectory extraction*

3.2.1.1 Extracting lateral and longitudinal trajectory

The available SV CAN speed in the time-series data was not sampled at the same frequency as other time-series data. This meant that, for some timestamps, there were 'NaN' values. A linear interpolation was therefore made to estimate the speed for all time-stamps, as seen in figure 3.6a. The distance travelled by the SV was then estimated through integrating the CAN speed, providing the distance travelled since the start of the event $(0 - 30[s])$, as shown in figure 3.6b. The longitudinal distance travelled by the POV was then calculated using (2.2).

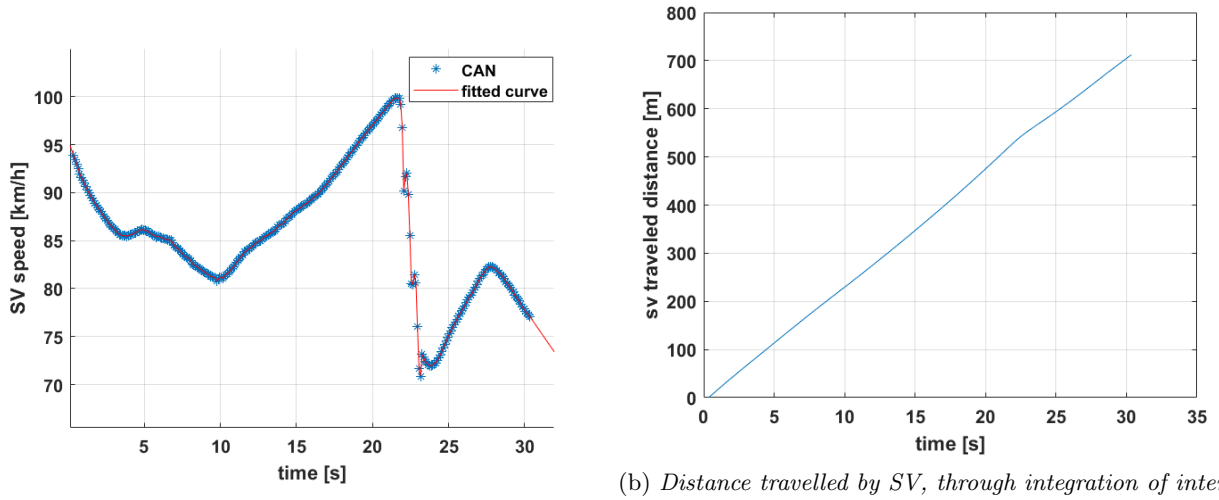

(a) *Interpolation of CAN speed*

(b) *Distance travelled by SV, through integration of interpolated speed*

Figure 3.6: *Steps of calculating the distance travelled by SV (event 1)*

A preliminary trajectory and the position of the lanes could now be plotted, as shown in figure 3.7, where the Global X axis measures the distance travelled; by both the SV and POV; since the start of the manoeuvre as defined in figure 2.9. The lane center was calculated as described in 2.3 and added to the same figure. Note however that the lateral distance on the Y axis is still relative to the SV, meaning that 0 is the center of the SV and not the lane. As a result, the left and right lane lines do not look straight. This is a result of the SV moving laterally in the target lane during the event.

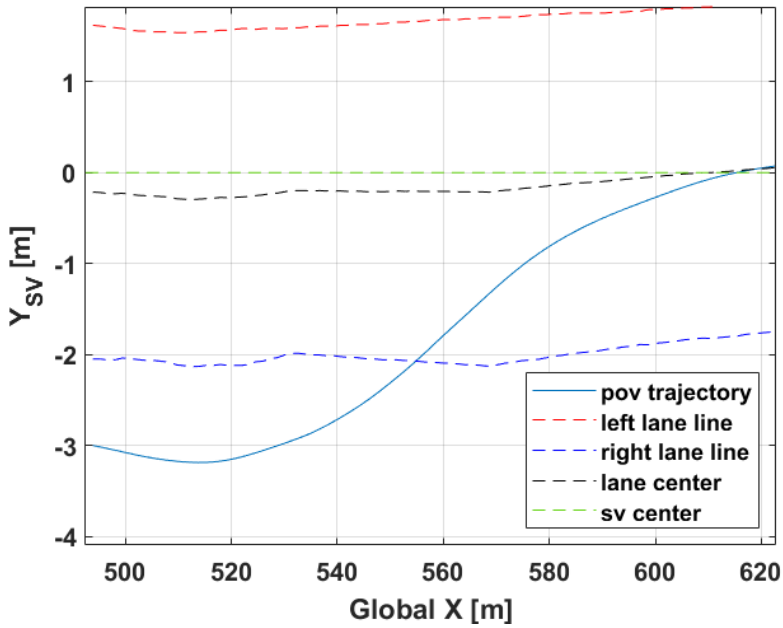

Figure 3.7: *Preliminary trajectory for event 1 where $Y_{sv} = 0$ is the center of the SV (event 1)*

The offset between the SV and lane center was calculated as using (2.4). This allowed for plotting the lateral distance with reference to the lane center. This is shown in Figure 3.8 where the complete trajectory of the event has been plotted in the global coordinate system defined in 2.9. On the Y axis is the lateral distance to the lane center and on the X axis is the longitudinal distance travelled since the start of the annotation. In

this representation, the trajectories of the POV and the SV are clear. One could also see how the SV moved towards the left of the target lane as the POV initiated the lane change manoeuvre as the driver of the SV became alerted by the move. It is valuable to note that, even though the trajectories of the POV and SV intersect at $\approx 620[m]$, the vehicles do not collide since they did not reach this distance at the same point in time.

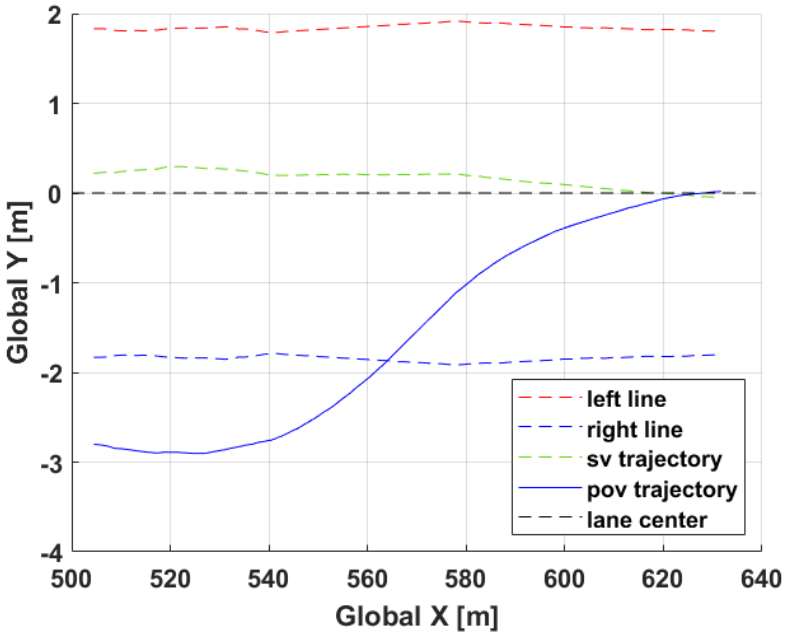

Figure 3.8: *Trajectory of SV and POV with reference to the global coordinate system, (event 1)*

From this representation, the POV lateral speed the $V_{Y,pov}$, longitudinal speed $V_{X,pov}$ and the SV lateral speed $V_{Y,sv}$ were calculated as described in section 2.3.1.3.

3.2.2 Defining Start and End of lane change

The algorithm described in section 2.3.2 was implemented in Matlab using the POV lateral speed and lateral distance to the lane center; $V_{Y,pov}$ and $Y_{LC,pov}$; in order to extract the: start time, end time, duration of the manoeuvre and categorise the lane change type; given the trajectory plotted in 3.8.

The signal $V_{Y,pov}$ was noisy and, therefore, a moving average filter was applied to the signal to smoothen the noise, as shown in figure 3.9a for event 1. The detected points for start and end of manoeuvre are plotted on the trajectory in figure 3.9b. This event was labelled as 'single lane change'.

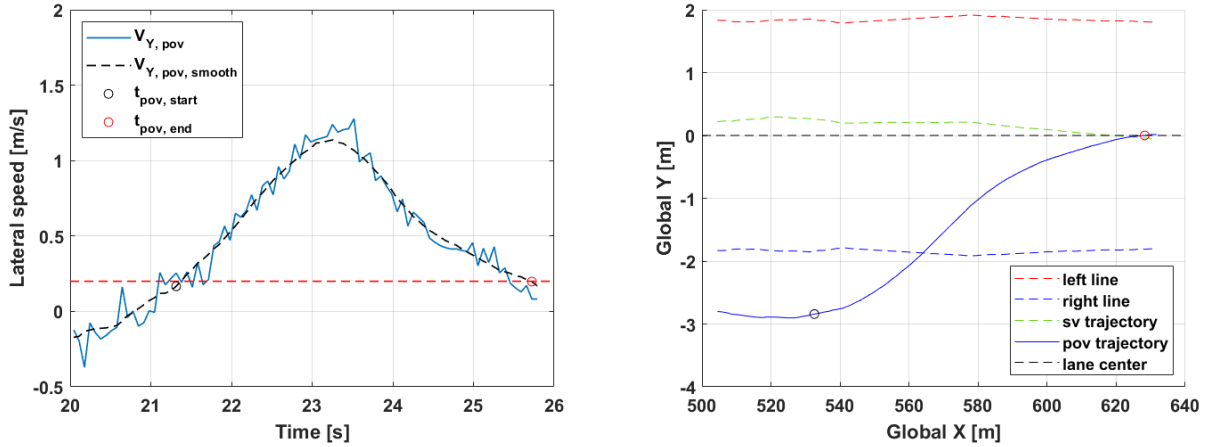

(a) *Defining start and end based on lateral speed* (b) *Start and end points in global trajectory*

Figure 3.9: *Detected start and end of a 'single lane change' manoeuvre (event 1)*

As seen in figure 3.9, the peak of lateral speed $V_{Y,pov,smooth}$ is at $\approx 23.5[s]$. The start time $t_{pov,start}$ is identified as the time where $V_{Y,pov,smooth}$ crosses the trigger threshold ($0.2[m/s]$) before $23.5[s]$, while the end time $t_{pov,end}$ is identified as the time $V_{Y,pov,smooth}$ is below the trigger threshold.

This method seems to identify the start and end of the manoeuvre correctly when the peak of the lateral speed is clear. This was not the case for all events, as shown in figure 3.10 for a *'hidden start'* lane change, where the $V_{Y,pov,smooth}$ never falls below the trigger value from the start of the manoeuvre, as seen in figure 3.10a. The most common cause for *'hidden start'*s was that the POV initiated the lane change manoeuvre at $\approx 40[m]$ from the SV: in these cases, the POV appeared very small in the image frame and consequently, errors in the annotation of the POV occurred. In such cases, the actual start time of the manoeuvre is not really captured. As a result, the event duration time was deemed inaccurate, because the start of the annotations is considered to determine the start of the lane change. This was also true for events labelled *'hidden end'*, as seen in figure 3.11. The most common cause for *'hidden end'* was that the video footage ended before the POV stabilised in the lane, capturing only part of the manoeuvre.

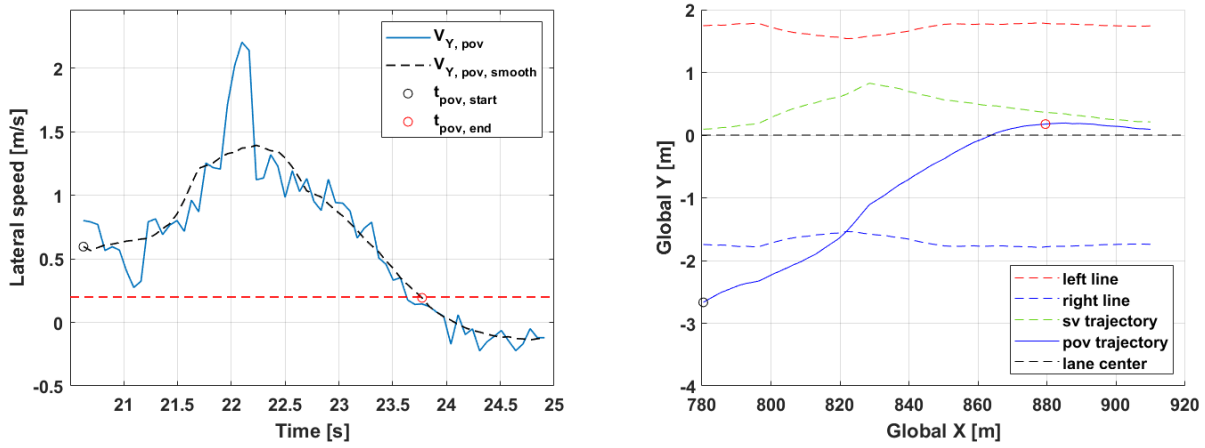

(a) *Defining start and end based on lateral speed* (b) *Start and end points in global trajectory*

Figure 3.10: *Detected start and end of a 'single lane change' manoeuvre with 'hidden start' (event 2)*

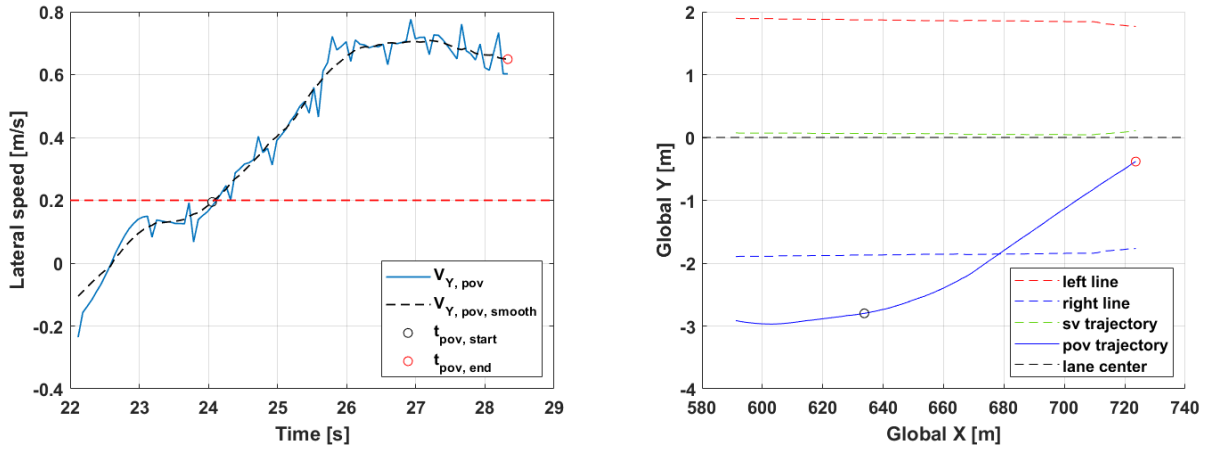

(a) *Defining start and end based on lateral speed* (b) *Start and end points in global trajectory*

Figure 3.11: *Detected start and end of a 'single lane change' manoeuvre with 'hidden end' (event 36)*

Other lane change types included *'double lane change start'* and *'double lane change end'*. All identified lane change types are shown in figure 3.12. In figure 3.12a, it is clear how events labelled *'hidden start'* represented a large portion of the annotated events. For these events, the duration was inaccurate. In total there were only 26 out of 57 annotated events that were both labelled as *'single lane change start'* and *'single lane change end'* and could be used for the statistical modelling.

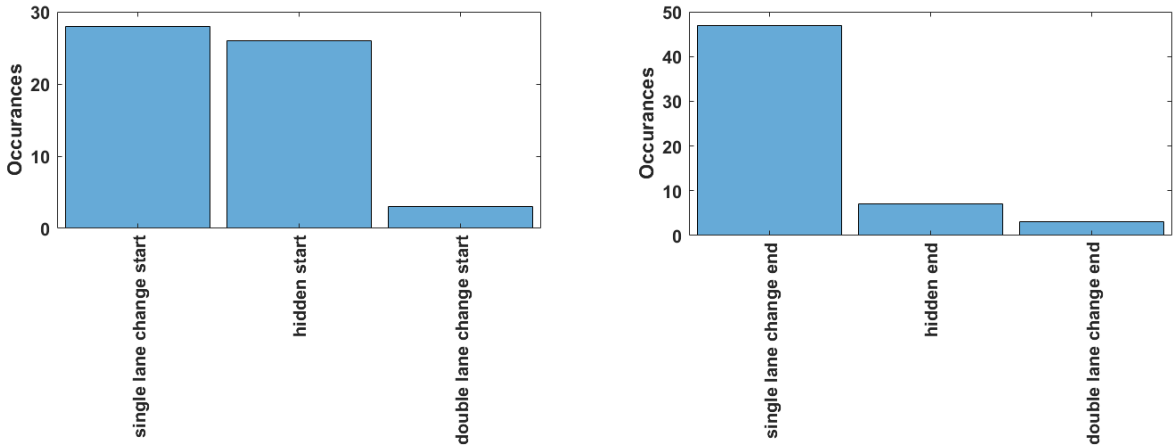

(a) *Start type* (b) *End type*

Figure 3.12: *All detected lane change types for the 57 annotated events*

3.2.3 Parameterising trajectories

After the complete trajectory for each event was extracted, the lateral and longitudinal trajectories were parameterised using ridge regression, as explained in section 2.3.3. This was implemented as a function that, given a trajectory like in figure 3.8 with the start and end time of the manoeuvre, would output the ridge reconstruction. This was done for all 57 annotated events. Figure 3.13 shows the result for event 1. The trajectory and the corresponding Ridge regression are also plotted on the global axis in figure 3.14, where it is apparent that the ridge reconstruction captures the trajectory of the event with good accuracy.

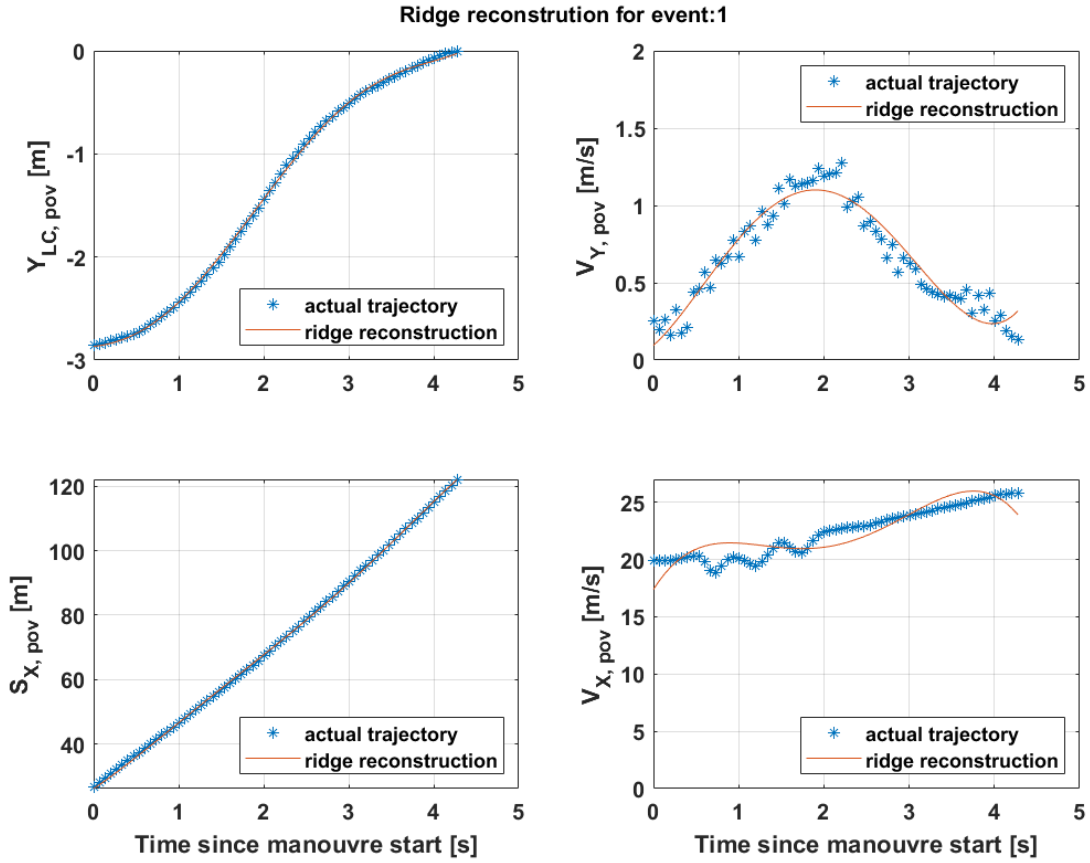

Figure 3.13: *Ridge estimation of trajectory (event 1)*

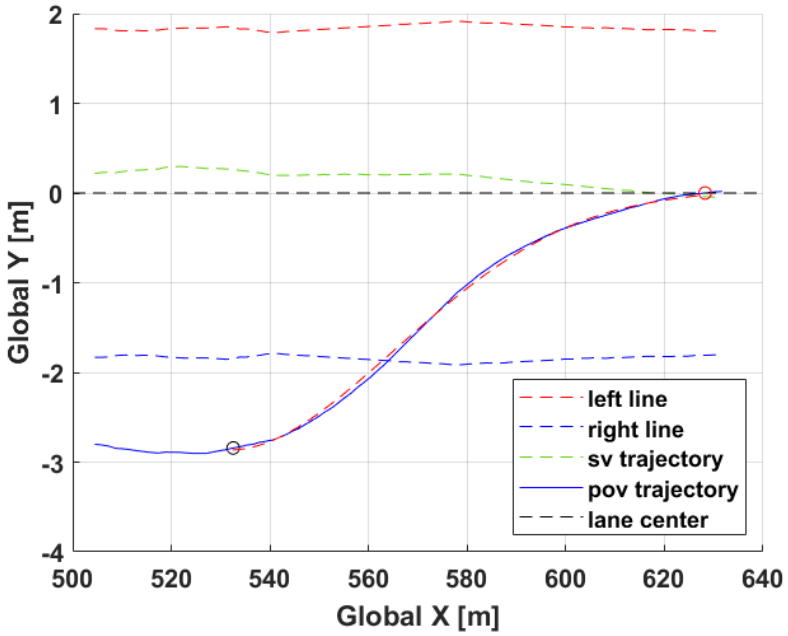

Figure 3.14: *Ridge estimation plotted in global coordinates (event 1)*

3.3 Uncertainty modelling

There were a total of 10 events that were annotated by all five annotators. Event 1 was excluded from the uncertainty modelling to test the uncertainty models of the lateral and longitudinal errors, while events (2-10) were used to train the models. In one of these events however, the POV was out of the frame for part of the manoeuvre. This event was initially chosen to investigate how differently the annotators would annotate such an event. It was found that there were large variations between the annotators and this event was therefore omitted from this analysis. This meant that only 8 events (2-9) were used to train the linear regression models used to estimate the uncertainty for the lateral and longitudinal range errors. The uncertainty of the models was evaluated using the standard deviation of the errors across users. Only event 1, is presented in detail in this section to showcase how the uncertainty was calculated.

3.3.1 Uncertainty of $R_{X,pov}$

In figure 3.15 the longitudinal distance annotated by the five annotators and the corresponding average of the annotations are plotted against time. As mentioned in 2.2.1.2, the annotators had the ability to manually remove any potential offset between the radar data and the tool output longitudinal range using the '+' and '-' keys. The offset correction was not considered because the purpose of this comparison was to assess differences in the annotation of the bounding box between different annotators and how these differences affected the results.

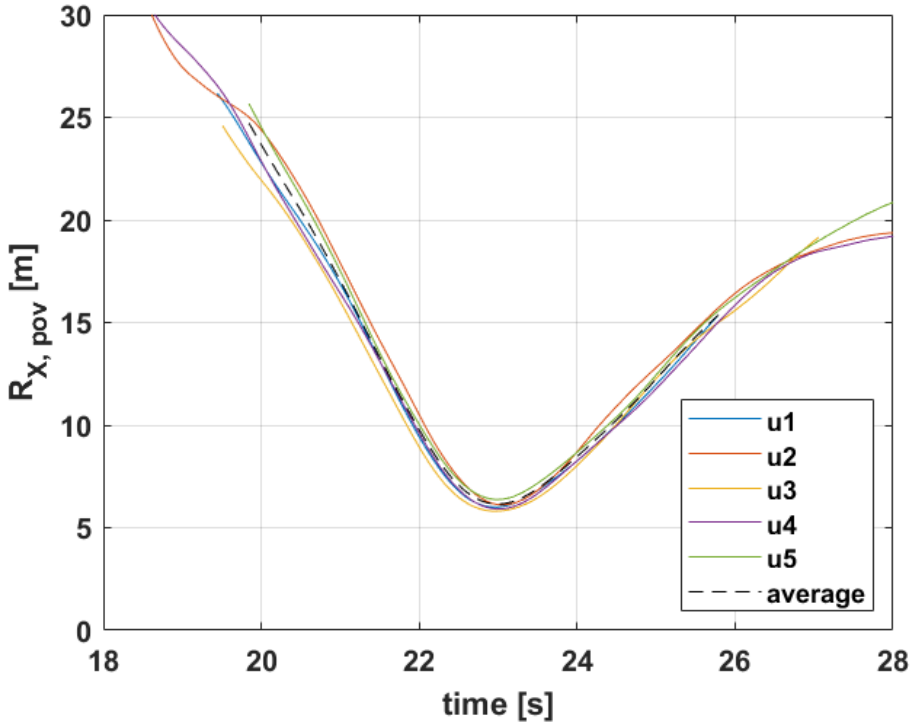

Figure 3.15: *Comparison of the longitudinal range between all five annotators (event1)*

As seen in figure 3.15, all annotations converge to the same minimum value of $\approx 6[m]$ and that this minimum occurred at the same time of $\approx 23[s]$. Upon first inspection, these results were promising showing small variation in how the users defined the bounding box around the POV rear. Note that the average of all 5 users seems to start at $\approx 20[s]$ and end at $\approx 26[s]$. This is simply because not all annotators annotated the same number of frames, and hence the annotation lengths are slightly different. The important part is that the critical manoeuvre was captured from the start.

The error of each user compared to the average is plotted in figure 3.16 against the longitudinal range. The standard deviation and mean of the error for this event are plotted in figure 3.17. These values are tabulated in table 3.2 for all 9 events separately.

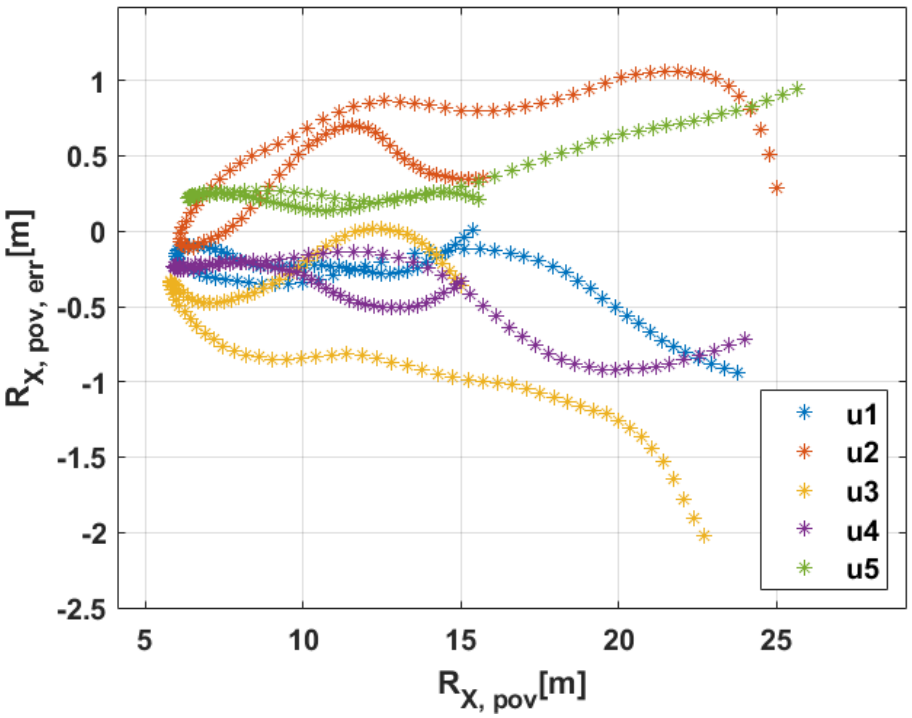

Figure 3.16: *Longitudinal range error of all five annotators (event 1)*

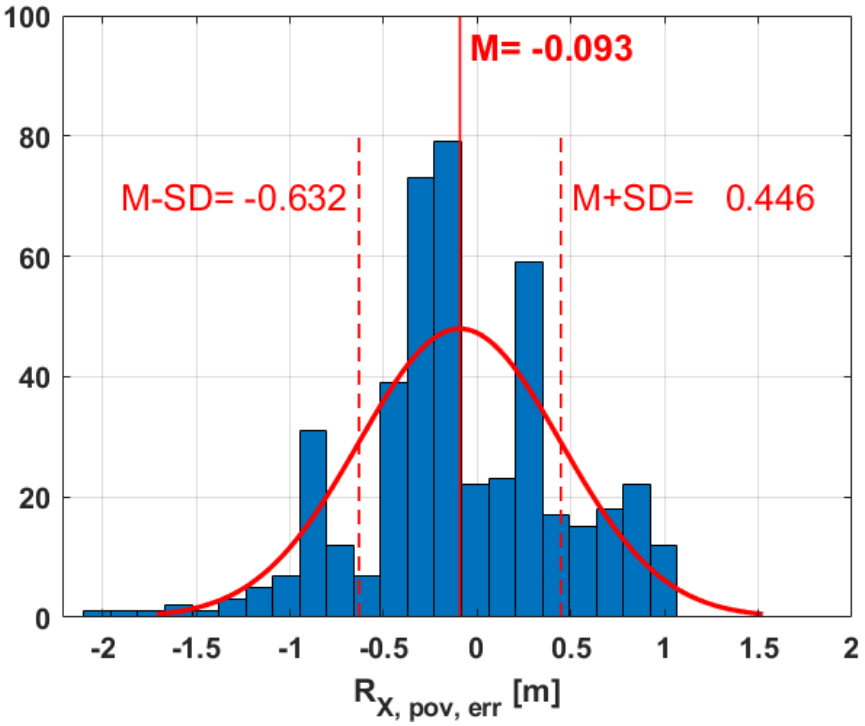

Figure 3.17: *Distribution of the longitudinal range error with mean (M) and standard deviation (SD) (event 1)*

Event	SD [m]	M [m]
1	0.538	-0.093
2	0.368	-0.141
3	0.528	-0.192
4	1.356	-0.638
5	0.273	-0.156
6	0.535	-0.240
7	0.415	-0.059
8	0.628	-0.245
9	0.993	-0.188

Table 3.2: Standard deviation (SD) and mean (M) of the longitudinal range error

In table 3.2, event 4 has a noticeably high standard deviation and mean values compared to the other events, where the mean value is almost negligible. This is due to this event being more difficult to annotate since the POV at the start of the manoeuvre was far from the SV and remained relatively far away during the entire event, while moving at a high relative speed. This caused high variance between different annotators. Nevertheless, it was chosen to neglect the mean values of the errors to simplify the uncertainty estimation. This was done as time did not allow for more accurate modelling of the uncertainty.

In figure 3.16, the manoeuvre start is at $\approx 20[m]$ where the longitudinal error is at its highest value of $\approx \pm 2[m]$. From this point, as the longitudinal range decreases and the POV moves closer to the POV ($\approx 5[m]$), the error decreases. This is simple a result of the POV being larger in the video frame when it is closer, making it easier to define a bounding box around the rear width. However, after the longitudinal range reaches its minimum at $\approx 5[m]$ and starts to increase again, the longitudinal range error seems to be lower at $\approx \pm 0.5[m]$. This is a result of the fact that after the longitudinal range has reached its minimum, the POV would have also moved laterally in-front of the SV. This means that towards the end of the manoeuvre, as the POV is in the target lane and directly in-front of the SV, the longitudinal range error is less affected by the longitudinal range. This result implies that the longitudinal range error is not only dependent on the longitudinal range,

but also on the lateral range.

This emphasised the need to model this error as a function of both the longitudinal and lateral ranges instead of only the longitudinal range. This was done using a linear regression model with the standard deviation of longitudinal range errors SD_X as observations; the average longitudinal and lateral ranges $R_{X,pov,avg}$ and $R_{Y,pov,avg}$ as predictors; as described in section 2.4.1.1. The model coefficient matrix a_X is shown in (3.1). With the developed model, the standard deviation for one annotator was calculated, as shown in figure 3.18. The uncertainty is shown in the figure as dotted lines with ± 2 standard deviation. This means that about 95% of all data-points should be within these ranges, with the other 5% equally scattered above and below these limits. The average longitudinal range of all 5 annotators is also plotted. There, it is apparent that the average of all 5 users is within the 95% confidence interval for the entire duration, which means that the model captured the uncertainty.

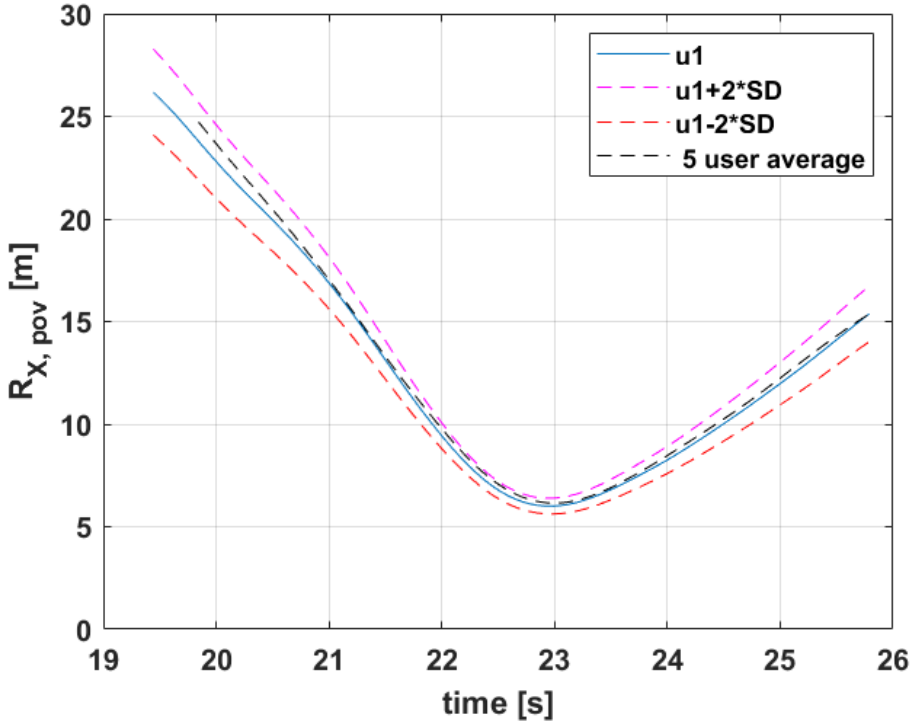

Figure 3.18: *The estimated longitudinal range uncertainty of one annotator using 2 standard deviations (SD) (event 1)*

$$a_X = \begin{bmatrix} 0.0440 & 0.0353 \end{bmatrix} \tag{3.1}$$

To compare how well this model captured the uncertainty for all annotators, the uncertainty of the average longitudinal range $R_{X,avg}$ was calculated. This is shown as the shaded area in figure 3.19. In this figure, it is apparent that $R_{X,pov}$ of all annotators remains within the shaded area most of the time. This suggest that using this model to calculate the uncertainty of one annotator, then one can be certain that the uncertainty of said annotator will remain within 2 standard deviations of the average, most of the time. This is also supported by the result in figure 3.18.

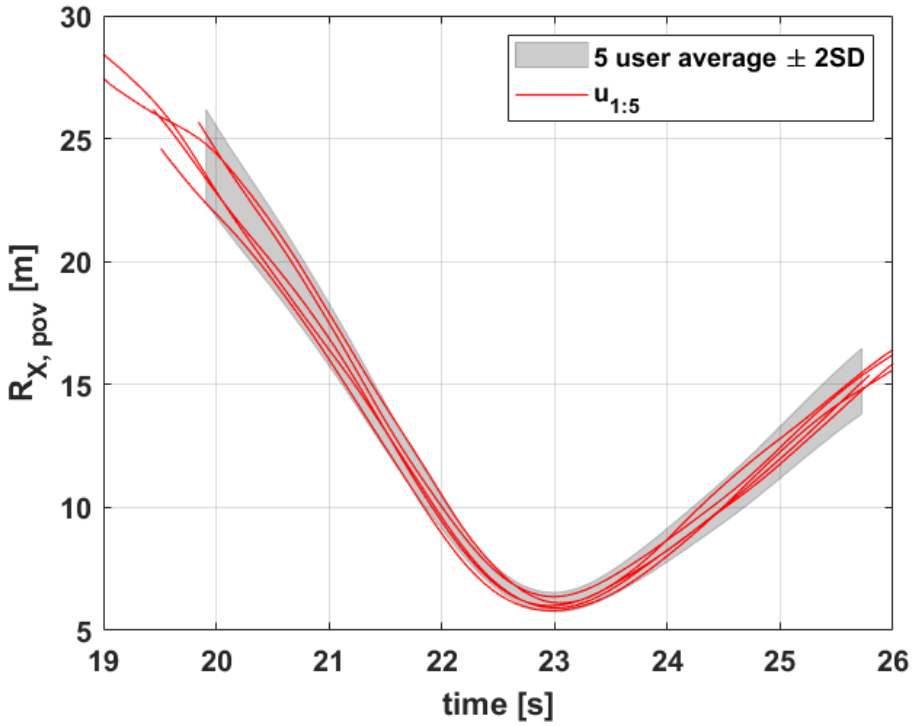

Figure 3.19: *The estimated longitudinal range uncertainty for the mean of all annotators (event 1)*

3.3.1.1 Uncertainty of $R_{Y,pov}$

In figure 3.20 the lateral distance of all five annotators and the corresponding average are plotted. In this figure, it is clear how the difference between the annotators is large during the start of the annotation at $\approx 20[s]$. Negative lateral range indicates that the POV is to the right of the SV and a lateral range of $0[m]$ indicates that the POV is directly in front of the SV. Hence, the event shown in the figure is a left lane change. The lateral error of each user compared to the mean is plotted in figure 3.21 against the longitudinal range. The distribution of the lateral range errors is plotted in figure 3.22. The values of the mean and the standard deviations of the errors for the 9 events are reported in table 3.3.

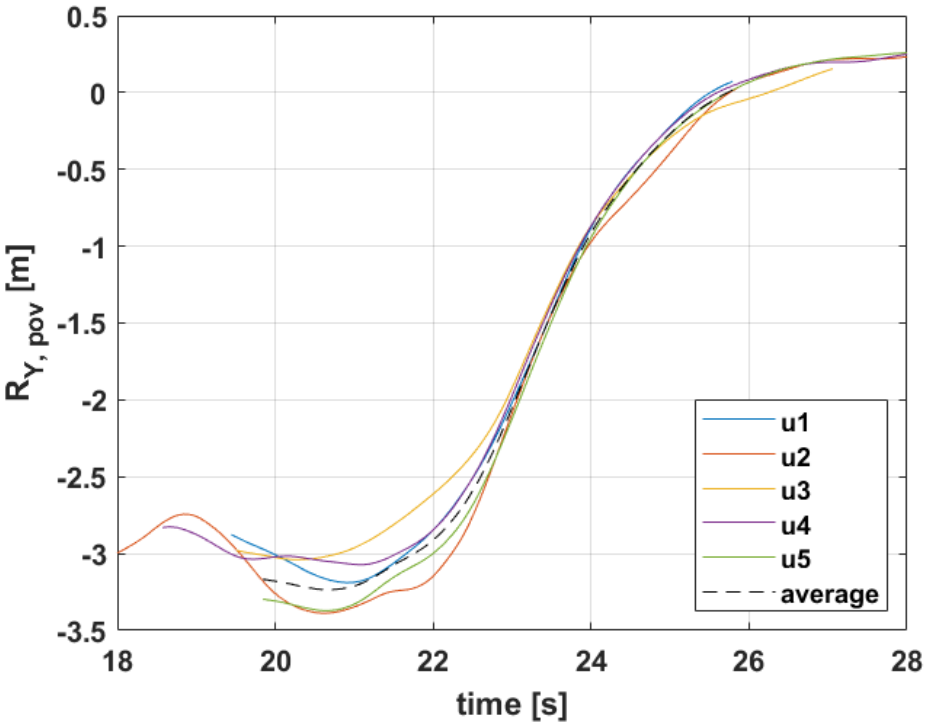

Figure 3.20: *Comparison of the lateral range between all five annotators (event 1)*

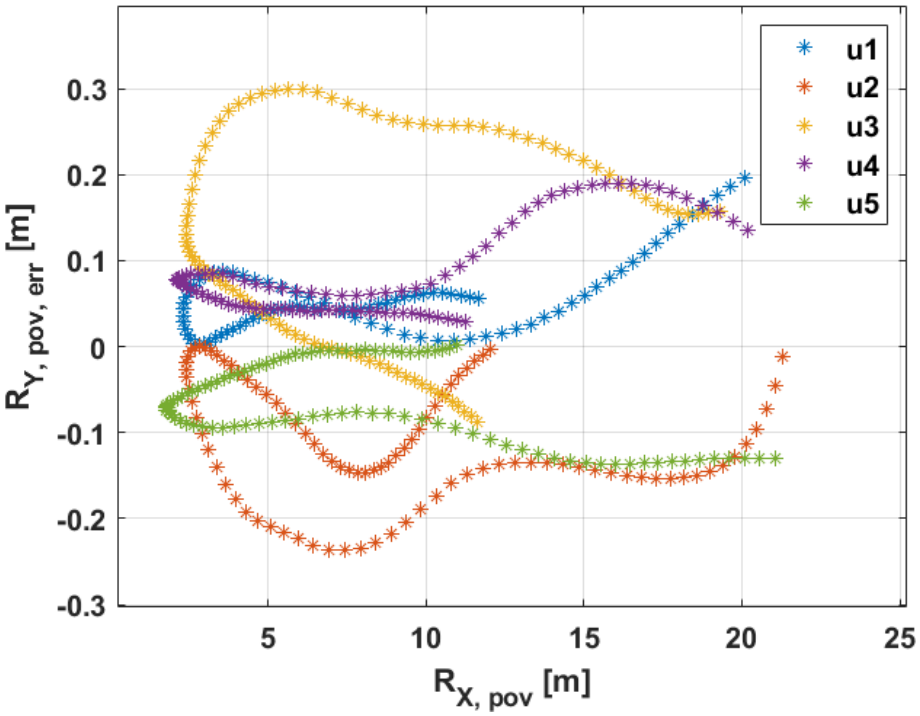

Figure 3.21: *Lateral range error of all five annotators (event 1)*

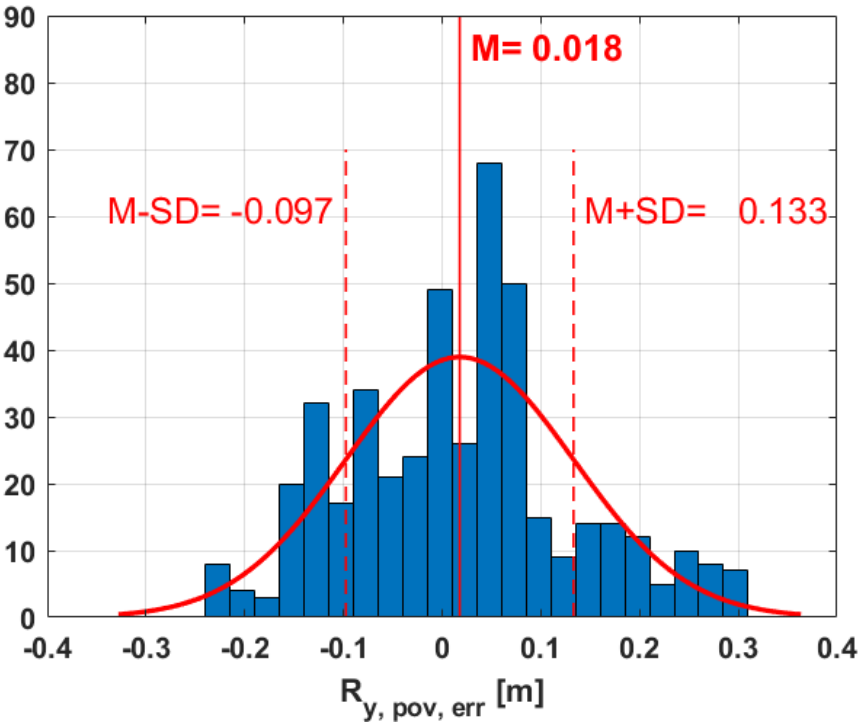

Figure 3.22: *Distribution of the lateral range error with mean (M) and standard deviation (SD) (event 1)*

Event	SD [m]	M [m]
1	0.115	0.018
2	0.057	0.015
3	0.153	0.047
4	0.120	-0.054
5	0.073	0.027
6	0.246	0.093
7	0.024	-0.000
8	0.060	0.0138
9	0.156	-0.021

Table 3.3: Standard deviation (SD) and mean (M) of the lateral range error (event 1)

In table 3.3, event 6 has a noticeably high standard deviation and mean values compared to other events. This event was special since it was a double lane change start: the POV was two lanes to the right of the SV before commencing a left lane change. This meant that it was just on the edge of the image frame, where the POV width was partially hidden due to the viewing angle. It is also apparent in table 3.3 that the mean value of the error for all events is small. It was therefore estimated to be 0 to simplify the uncertainty estimation, as was done for the longitudinal range error previously.

In figure 3.21, the manoeuvre start is at $\approx 20[m]$, where the lateral error is $\pm 0.2[m]$. The error stays within this threshold for 3 of the users until the longitudinal distance reaches its minimum value of $\approx 5[m]$, after which point the lateral range error decreases to $\approx \pm 0.1[m]$. Again, this is a result of the POV being directly in-front of the SV towards the end of the manoeuvre. The lateral range error would therefore also need to be modelled as a dependant variable of both the longitudinal range and the lateral range.

Another interesting finding by studying 3.21 is that the lateral range error seems to reach its largest value at the middle of the manoeuvre where the longitudinal range is $\approx 5[m]$ for two of the annotators. This means that as the POV is changing lane, the lateral error is at its highest value of $\approx \pm 0.3[m]$. This suggests that

maybe the POV lateral speed should also be included in the uncertainty estimation of the lateral range error. However, due to the limited time of the project, this was not investigated.

Instead, the lateral range error was modelled as a function of the lateral and longitudinal ranges, as was done for the longitudinal range error. This was done using a linear regression model with the standard deviation of longitudinal range error SD_Y as observations; the average longitudinal and lateral ranges $R_{X,av}$ and $R_{Y,avg}$ as predictors; as described in section 2.4.1.1. The model coefficient matrix a_Y is shown in (3.2). The developed model was then used to estimate the standard deviation for one annotator, as seen in figure 3.23. The uncertainty is shown in this figure as the two dotted lines at ± 2 standard deviations, as was done for the longitudinal range in the previous section. In this figure, it is apparent that the average of all annotators is within the 95% confidence interval, which means that this model captured the uncertainty. It is apparent from this figure that the uncertainty is at its largest at $\approx 21[s]$, which is about that the POV initiated the lane change manoeuvre. At this point, where the POV is at a longitudinal range of $\approx 20[m]$ (see figure 3.18), the uncertainty in the lateral range is $\approx \pm 0.5[m]$. This uncertainty then continues to decrease as the POV continues the manoeuvre until $\approx 24[s]$, after which point it increases slightly as the POV moves further away.

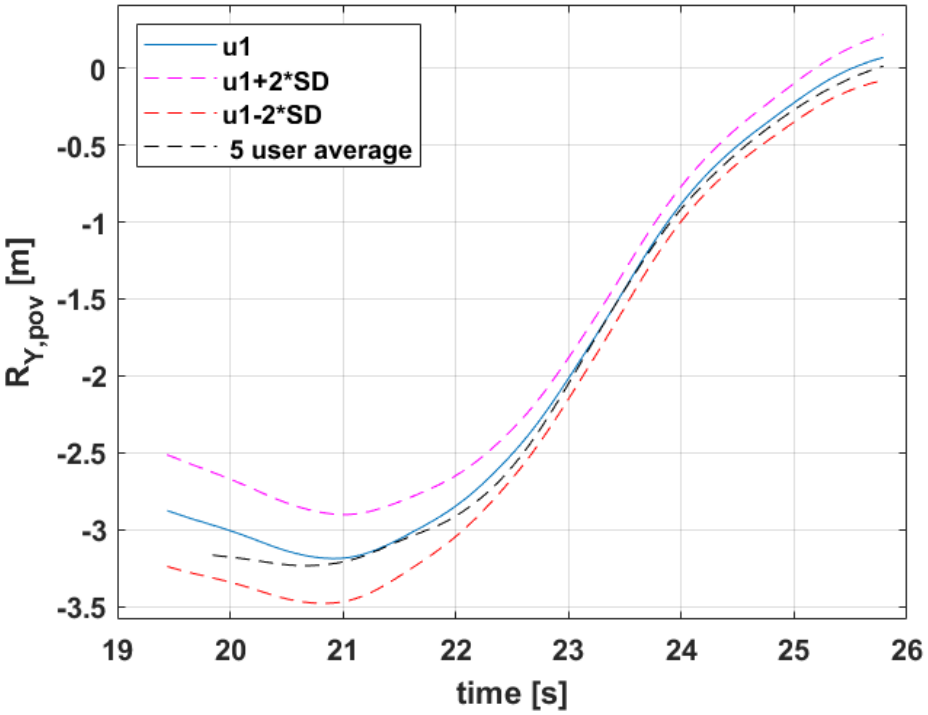

Figure 3.23: *The estimated lateral range uncertainty of one annotator (event 1)*

$$a_Y = \begin{bmatrix} 0.0049 & 0.0185 \end{bmatrix} \tag{3.2}$$

To compare how well this model captured the uncertainty for all annotators, the uncertainty of the average lateral range $R_{Y,pov,avg}$ was calculated, as was done in the previous section for the longitudinal range. This is shown as the shaded area in figure 3.24. In this figure, the lateral range $R_{Y,pov}$ remained within the shaded area for most of the time. Again, this suggests that using this model to calculate the uncertainty of one annotator, then the uncertainty of said annotator should remain within 2 standard deviations of the average, most of the time.

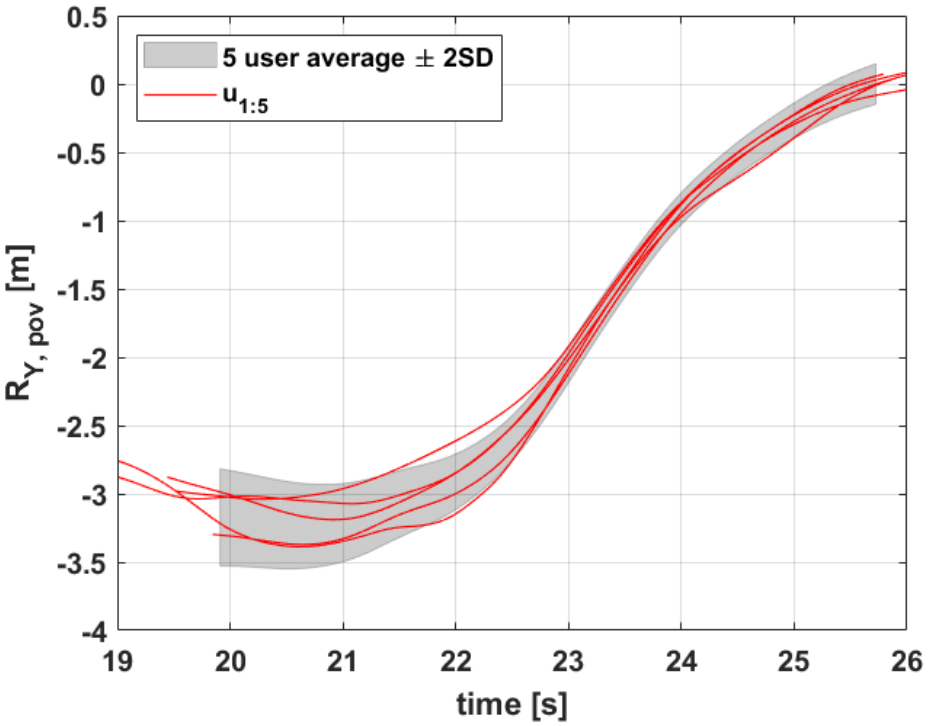

Figure 3.24: *The estimated lateral range uncertainty for the mean of all annotators (event 1)*

3.3.1.2 Uncertainty of $Y_{LL,sv}$ and $Y_{RL,sv}$

In figure 3.25, the lane placement for all 5 annotators and the corresponding average are plotted. In this figure, there is no clear trend of how the lanes are annotated by different users other than that the variation seems to be larger between $22 - 24[s]$, which is where the SV moved towards the left lane line during the manoeuvre to get further away from the POV. This is seen as the average left lane line gets closer to the SV. As explained in section 2.4.2, the lanes were assumed to be two parallel lines stretching along the roadway. This meant that there was no measurable longitudinal component to model error. The error was therefore only compared to the SV lateral distance to respective lanes $Y_{LL,sv}$ and $Y_{RL,sv}$. In figure 3.26 the errors are plotted against the lateral distance between the SV and the lanes. From the figure, it is difficult to notice a clear trend. The mean and standard deviations of the errors were calculated and plotted in figure 3.27. As can be seen in figure 3.27a, the left lane has higher error values compared to the right lane in figure 3.27b. The larger error in the left lane could be attributed to the lane line on the left not being clear during some part of the manoeuvre. However, it is clear in figure 3.27 that the mean and standard deviation values of the errors for both the left and right lanes are small, which is preferable. This is also true for all 9 events, as seen in table 3.4. This indicates that the user variation on average is not large for $Y_{LL,sv}$ and $Y_{RL,sv}$ and can therefore be neglected.

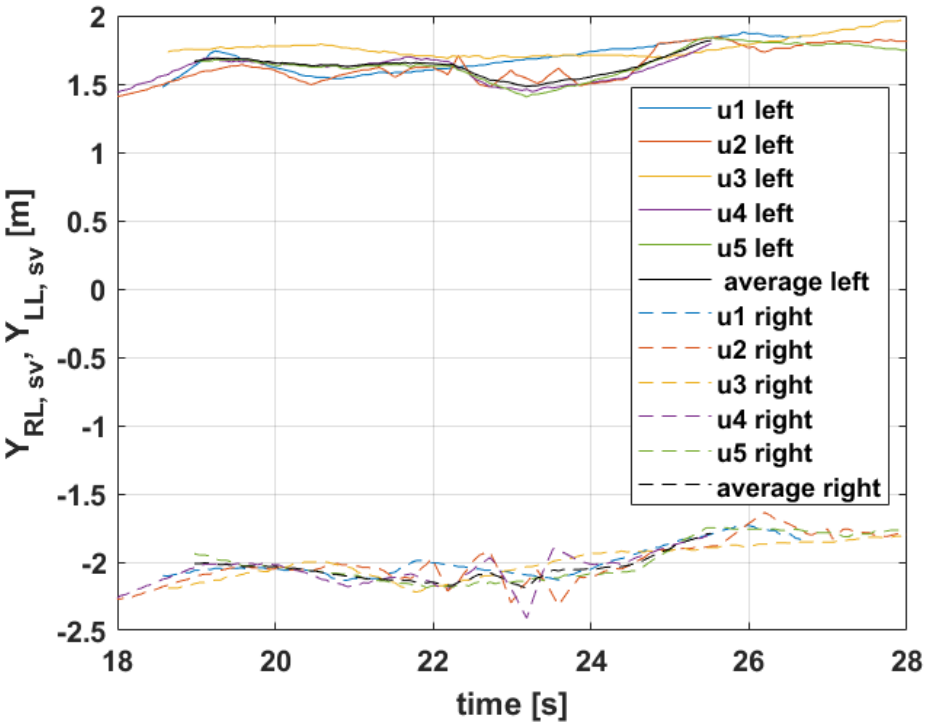

Figure 3.25: *Comparison of distance to left and right lanes for all users (event 1)*

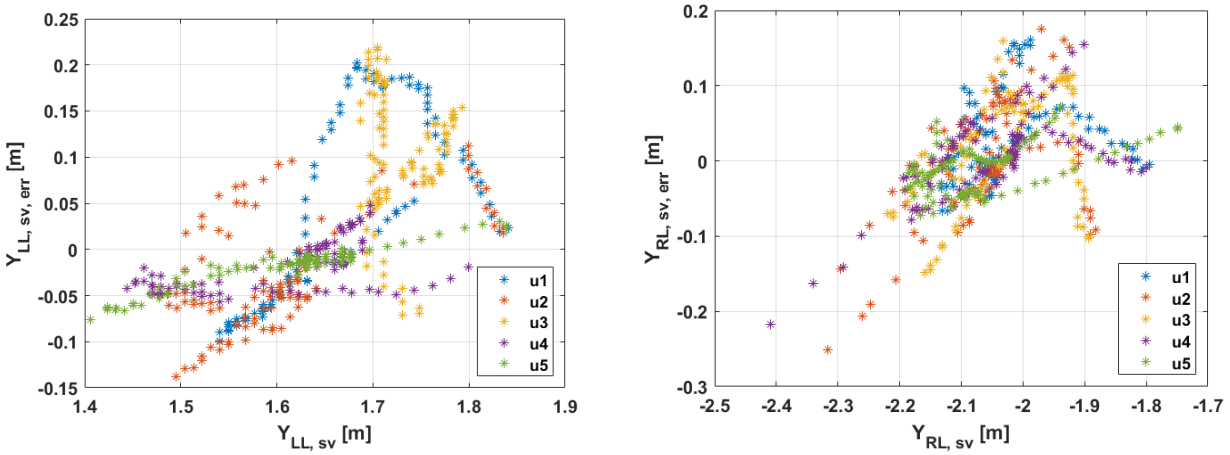

(a) *Lateral distance to left lane error*

(b) *Lateral distance to left lane error*

Figure 3.26: *Lane line error of all 5 annotators (event 1)*

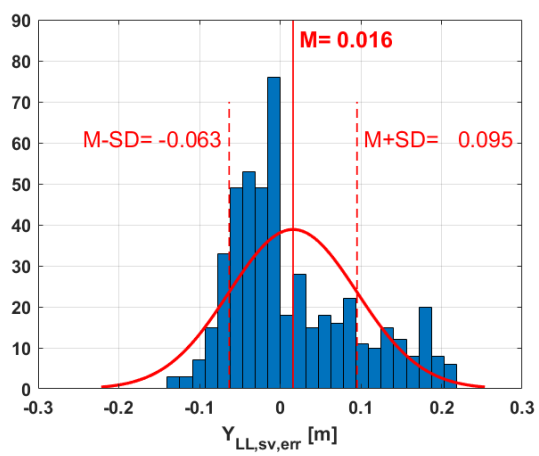

(a) *Distribution of the left lane error*

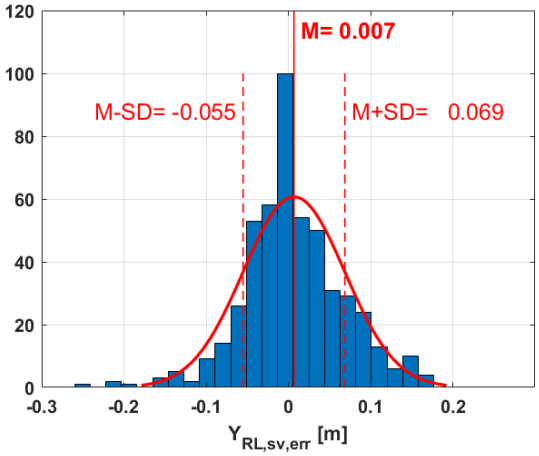

(b) *Distribution of the right lane error*

Figure 3.27: *Lane line error distributions with standard deviation (SD) and mean (M) (event 1)*

	Left lane line		Right lane line	
Event	SD	M	SD	M
1	0.079	0.016	0.062	0.007
2	0.041	0.003	0.095	0.028
3	0.041	0.006	0.081	0.0171
4	0.070	0.000	0.067	-0.007
5	0.062	0.004	0.099	0.009
6	0.048	0.010	0.090	-0.003
7	0.075	0.009	0.048	-0.010
8	0.073	-0.012	0.074	-0.024
9	0.069	-0.006	0.072	0.0127

Table 3.4: Standard Deviation and Mean of lane errors for all 9 events

4 Discussion

The aim of this thesis was to develop a statistical model of lane-change manoeuvres through studying a data-set of 1191 critical lane changes collected through the SHRP2 NDS. The kinematics of the lane-change manoeuvres were to be extracted using an annotation tool that was developed for this purpose as part of a previous project. After careful selection, 86 events were deemed suitable for annotation. This raised concern that the number of annotated events were too few to make any credible statistical modelling of the completed lane-change manoeuvre. As the number of usable events were believed to be considerably larger, the initial plan was to hire one or two part-time annotators to aid the annotation process. This was ultimately never done, due to administrative reasons (including Covid19). Instead, the supervisors of this project and another project assistant supported the annotation process. Initially, having five different annotators introduced a higher degree of complexity to the analysis, due to the difficulties in keeping track of the events annotated by each person and the risk of overwriting each-others annotations.

However, the possibility to get the output of several annotators allowed for better understanding of the variation between different annotators. Based on the output obtained from the events annotated by everyone, it was found that the outcome of the annotations affected the variables extracted and the consequent modelling. Therefore, the scope of the thesis was redirected towards the preparation of the variables/parameters for the statistical modelling and the analysis of the uncertainty associated to the annotation process.

Before this was decided, the author had annotated a number of events and used them to develop methods for extracting the trajectory of the lane-change manoeuvres. This was done through combining the annotation output with time-series data available from the data-set.

This method produced reasonable results. In fact, the extracted trajectories look smoother compared to the trajectories extracted by Wang, Yang, and Hurwitz [22]. It is important to note that this method of extracting the trajectory assumes that the lanes are straight, meaning that lane curvature is not captured. An attempt was made to estimate the lane curvature using the accelerometer and gyroscope data that is available in the time-series data. The values obtained using this method were however not reasonable due to the lateral acceleration signal being either noisy, offset or missing for most events.

Moreover, the extracted trajectories were assessed by watching the video for the event and visually evaluating if the trajectory was reasonable. This shortcut was taken due to the limited time available for the thesis work, but future work should improve the assessment of the POV trajectory: one option would be to chose an event, like event 1 where the radar data is available for the entire manoeuvre, and identify the target ID of the POV in the radar data for the entire event. The radar data could then be used to reconstruct the trajectory and compared to the one extracted using the annotation tool.

The algorithm developed to define the start and end of a lane change and classify the lane change type functioned as intended. Its limitation was that it only relied on the POV lateral speed $V_{Y,pov}$ to detect the start and end time of the manoeuvre. Since $V_{y,sv}$ was calculated through differentiation of the lateral position $Y_{LC,pov}$, which was gained through manual annotation, this signal was noisy. As a result, for some cases $V_{Y,pov}$ would instantaneously fall below the trigger value, which would provide an inaccurate start or end time for a manoeuvre. Simply applying a moving average filter was a quick solution and did provide reasonable results. However, more advanced filtering algorithms could be applied to this signal. Parameterising the trajectory using ridge regression was also successful. Even though the parameterised trajectory was never part of the analysis, it was implemented in preparation for the statistical modelling of the lane-change. All the functions for extracting the manoeuvre kinematics and parameters the annotation output have been developed so that it is simple to add more annotations and get the output presented in section 3.2.

As no annotators were hired, the annotation process took longer than initially planned. This was also impacted by the outbreak of the Covid-19 pandemic, which limited access to the data as it was only available in secured rooms at SAFER. These limitations, along side the limited time of the project, resulted in only 56 events being annotated. Out of these, 10 were annotated by all five annotators. After analysing the 56 events using the trajectory extraction algorithm, it was found that the start and end of the lane-change manoeuvres were captured in only 26 of the 56 annotated events. This was further limiting since only completed lane-changes were to be considered for developing the statistical model of lane-changes. For comparison, Wang, Yang, and Hurwitz [22] had identified thousand of lane-changes with the similar criteria (for suitable lane-changes) using

a different data-set. This was what ultimately caused the aim of the thesis to be redirected to modelling the uncertainty of the different annotators using the 10 events that were annotated by all annotators. However, one event was excluded from this analysis due to it being unsuitable. In this event, the POV was outside the image frame for part of the manoeuvre. It was initially included as to investigate how different the output would be for such events. As it was later found, the variance in the output between the different annotators was too large, and this event was therefore excluded.

Two linear regression models to estimate the uncertainty of the longitudinal and lateral range outputs from the tool; $R_{X,pov}$ and $R_{Y,pov}$; were then developed using 8 of the 9 events. The last (event 1) was used to test how well these models captured the uncertainty of these measurements. It was found that these models did capture most the variation in $R_{X,pov}$ and $R_{Y,pov}$ between users. They did so while using several simplifications such as: assuming that the errors in these measurement are normally distributed and that the mean value of these errors are negligible. For the event 1, the uncertainties of both $R_{X,pov}$ and $R_{Y,pov}$ were largest at a range $R_{X,pov} \approx 20[m]$. At this point, the uncertainty in the longitudinal range was $\pm 2[m]$. This distance can be covered in less than $0.1[s]$ assuming a highway speed of $90[km/h]$. For the lateral range, the uncertainty was $\pm 0.4[m]$, which is less than 1/4 of a vehicle width, assuming that the width of the POV is $1.6[m]$. For reference, the width of a Fiat 500, which is a rather narrow vehicle, is $1.62[m]$. Both uncertainties decreased as $R_{X,pov}$ decreased. This indicates that the longitudinal range has a large impact on the uncertainties of $R_{X,pov}$ and $R_{Y,pov}$. The uncertainty models proposed in this thesis, although simple, allow for estimating the uncertainties of $R_{X,pov}$ and $R_{Y,pov}$ for events annotated by one annotator. They also showcase the reliability of this annotation method if is considered for future projects. The uncertainties in the left and right lane placements; $Y_{LL,pov}$ and Y_{RL_pov}; were evaluated through studying the standard deviation and mean value of the errors. It was found that these were small for most events, indicating that the annotators are consistent when defining the lane lines.

For the context of evaluating AV and ADAS functions, the exact trajectory of an event does not have to be captured. As long as the uncertainty of the complete trajectory is known; and is reasonable; then one can simulate a range of trajectories that are within the uncertainty bounds. These can then be used to evaluate different AV and ADAS functions. As was shown by Zhao et al. [21], simulations can be run for millions of tests for a fraction of the cost of FOTs. From the limited number of annotated events, it is concluded that this method of annotation should be suitable for this purpose.

Finally, developing the tool itself, not only for this project but also for potential upcoming work, has been an important part of this project. During the thesis work, the GUI of the tool was improved to facilitate the annotation process. As well, the keyboard controls that allowed for refining the POV placement were added. The list developed to keep track of the suitable events as well as which annotator did the annotation simplified the annotation and analysis processes.

Through making many minor improvements, the usability and stability of the tool was increased. However, there are still several areas where the tool can be improved, such as the distance calculation methods: the output of the tool seemed to provide a different value of the longitudinal range to the POV, compared to the value retrieved from the radar data. The short term solution adopted in this thesis was to allow the annotator to manually remove this offset via keyboard controls. However, a more stable solution should be found in the future, in order to ensure reliable estimation of the longitudinal range, also when the information from the radar (or other measurement units) is not used. Related to that, additional relevant future work stems from the need to adapt the current tool to other data-sets, where the camera parameters and available information might be different.

4.1 Limitations

The main limitation of this thesis project is represented by the low number of cases considered, compared to the initial plan. The reduction in the number of events - from the whole data-set of 1191 events to the 86 suitable events - is due to the defined criteria (see 2.1.2). This reduction was not only caused by the limitations of the annotation tool. Out of all events, 54% were of incident type *'side swipe'*, where the POV was almost completely beside the SV. In these cases, the POV rear was not visible in the video recordings, making tracking the POV not possible. However, since the radar unit is mounted at the front of the SV near the license plate, the POV was not detected by the radar either. Moreover, 36% of the 241 that were manually screened by the

author were motivated as either: *'Partial lane change'*, *'POV is a truck'* or *'SV changed lane'*. These were excluded as part of the initial scope of this thesis.

The data-set being only accessible at SAFER was also a limitation, albeit for an unpredictable reason. This was initially not a constraint, however, as the Covid-19 out-brake cased several restrictions and students were recommended to study from home, the author reduced the number of visits to SAFER, which effectively reduced the time available to work with the data. This, along side the fact that no external annotators were hired and the limited number of suitable events, meant that the scope of the thesis had to be redirected.

4.2 Future work

As previously mentioned, the annotation tool used in this project has several limitations. Before it can be considered for this type of annotation, the distance calculation methods have to be improved to account for the inaccuracy in the longitudinal range. Previous research has shown that estimating the longitudinal range to the POV through manually annotating the POV width in an image-frame can be done with an accuracy of $\pm 0.1[m]$ at $10[m]$ range and $\pm 4[m]$ at $30[m]$ range [27]. This is considerably better than the estimated longitudinal range gained from the annotation tool, which could be offset by $2[m]$ at $10[m]$ range when compared to the radar range. As previously mentioned, the short term solution adapted in this project was to have this offset removed by the annotators using keyboard controls.

Additional inputs to estimate the road curvature, as was done in the annotation tool used in Lee, Olsen, Wierwille, et al. [17], can also be added. This was done through allowing the annotator to fit a polynomial to the lane-lines and hence estimate the curvature. Moreover, the video player window could be made larger to make annotation easier. Finally, the uncertainty models presented in this thesis were developed using a limited number of events. Future development of this method could include more annotators, events and variables; potentially $V_{X,pov}$ and $V_{Y,pov}$; to model the uncertainty and get a better understanding of the uncertainty associated with this annotation method.

It is also valuable to note that the data-set used in this thesis was collected in the USA, meaning that any potential conclusion about driver behaviour can be limited to the geographical area and may not be representative of how drivers would behave in other locations.

References

[1] N. A. Stanton and P. Marsden. From fly-by-wire to drive-by-wire: safety implications of automation in vehicles. *Safety science* **24**.1 (1996), 35–49.

[2] F. Jiménez et al. Communications and Driver Monitoring Aids for Fostering SAE Level-4 Road Vehicles Automation. *Electronics* **7**.10 (2018), 228.

[3] R. Okuda, Y. Kajiwara, and K. Terashima. "A survey of technical trend of ADAS and autonomous driving". *Technical Papers of 2014 International Symposium on VLSI Design, Automation and Test*. 2014, pp. 1–4.

[4] S. Taxonomy. Definitions for terms related to on-road motor vehicle automated driving systems. *Society of Automotive Engineers (SAE): Troy, MI, USA* (2014).

[5] J. Fleetwood. Public health, ethics, and autonomous vehicles. *American journal of public health* **107**.4 (2017), 532–537.

[6] T. Litman. *Autonomous vehicle implementation predictions*. Victoria Transport Policy Institute Victoria, Canada, 2017.

[7] B. Färber. "Communication and communication problems between autonomous vehicles and human drivers". *Autonomous driving*. Springer, 2016, pp. 125–144.

[8] M. J. Cassidy and R. L. Bertini. Some traffic features at freeway bottlenecks. *Transportation Research Part B: Methodological* **33**.1 (1999), 25–42.

[9] J. Chovan et al. *Examination of lane change crashes and potential IVHS countermeasures. Final Report*. Tech. rep. 1994.

[10] M. Benmimoun et al. "Safety analysis method for assessing the impacts of advanced driver assistance systems within the European large scale field test euroFOT". *8th ITS European Congress*. 2011.

[11] F. Guo et al. Near crashes as crash surrogate for naturalistic driving studies. *Transportation Research Record* **2147**.1 (2010), 66–74.

[12] M. M. Minderhoud and P. H. Bovy. Extended time-to-collision measures for road traffic safety assessment. *Accident Analysis & Prevention* **33**.1 (2001), 89–97.

[13] J. Lundgren and A. Tapani. Evaluation of safety effects of driver assistance systems through traffic simulation. *Transportation research record* **1953**.1 (2006), 81–88.

[14] E. Donges. A two-level model of driver steering behavior. *Human factors* **20**.6 (1978), 691–707.

[15] I. Isaksson-Hellman and H. Norin. "How thirty years of focused safety development has influenced injury outcome in Volvo cars". *Annual Proceedings/Association for the Advancement of Automotive Medicine*. Vol. 49. Association for the Advancement of Automotive Medicine. 2005, p. 63.

[16] M. Lindman and E. Tivesten. A method for estimating the benefit of autonomous braking systems using traffic accident data. *SAE Transactions* (2006), 291–301.

[17] S. E. Lee, E. C. Olsen, W. W. Wierwille, et al. *A comprehensive examination of naturalistic lane-changes*. Tech. rep. United States. National Highway Traffic Safety Administration, 2004.

[18] N. Kauffmann et al. "What Makes a Cooperative Driver?" Identifying parameters of implicit and explicit forms of communication in a lane change scenario. *Transportation research part F: traffic psychology and behaviour* **58** (2018), 1031–1042.

[19] P. G. Gipps. A model for the structure of lane-changing decisions. *Transportation Research Part B: Methodological* **20**.5 (1986), 403–414.

[20] T. Toledo, H. N. Koutsopoulos, and M. E. Ben-Akiva. Modeling integrated lane-changing behavior. *Transportation Research Record* **1857**.1 (2003), 30–38.

[21] D. Zhao et al. Accelerated evaluation of automated vehicles safety in lane-change scenarios based on importance sampling techniques. *IEEE transactions on intelligent transportation systems* **18**.3 (2016), 595–607.

[22] X. Wang, M. Yang, and D. Hurwitz. Analysis of cut-in behavior based on naturalistic driving data. *Accident Analysis & Prevention* **124** (2019), 127–137.

[23] A. H. S. El Din et al. TME-180 Final report Variables extraction and trajectory reconstruction for modelling driver behaviour (2020).

[24] K. L. Campbell. *The SHRP 2 Natrualistic Driving Study: Adressing Driver Performance and Behaviour in Traffic safety*. `https://insight.shrp2nds.us/documents/shrp2_background.pdf`. [Online; accessed May-2020]. 2012.

[25] J. F. Antin. *Design of the in-vehicle driving behavior and crash risk study: in support of the SHRP 2 naturalistic driving study*. Transportation Research Board, 2011.
[26] T. A. Dingus et al. *Naturalistic driving study: Technical coordination and quality control*. SHRP 2 Report S2-S06-RW-1. 2015.
[27] J. Bärgman et al. Using manual measurements on event recorder video and image processing algorithms to extract optical parameters and range (2013).
[28] M. S. Shirazi and B. T. Morris. Trajectory prediction of vehicles turning at intersections using deep neural networks. *Machine Vision and Applications* **30**.6 (2019), 1097–1109.
[29] G. A. Seber and A. J. Lee. *Linear regression analysis*. Vol. 329. John Wiley & Sons, 2012.
[30] G. K. Uyanık and N. Güler. A study on multiple linear regression analysis. *Procedia-Social and Behavioral Sciences* **106**.1 (2013), 234–240.
[31] D. W. Marquardt and R. D. Snee. Ridge regression in practice. *The American Statistician* **29**.1 (1975), 3–20.
[32] A. E. Hoerl and R. W. Kennard. Ridge regression: Biased estimation for nonorthogonal problems. *Technometrics* **12**.1 (1970), 55–67.
[33] A. E. Hoerl et al. Application of ridge analysis to regression problems (1962).
[34] D. G. Altman and J. M. Bland. Standard deviations and standard errors. *Bmj* **331**.7521 (2005), 903.

Appendices

A Appendix 1

A.1 Usable event list

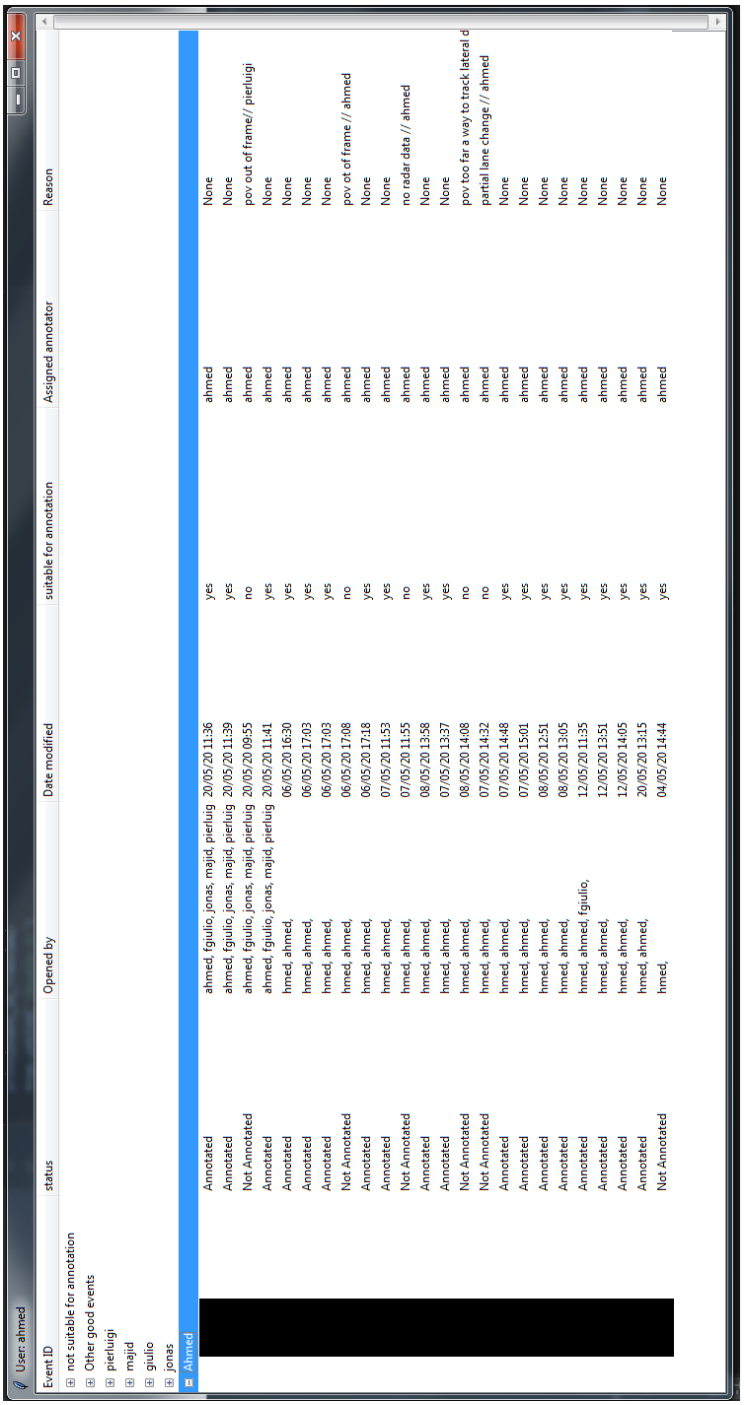

Figure A.1: *The developed list containing all filtered events and their assigned annotator*

A.2 Annotation tool guide

Intro

In this document, I will try and summarize how to control the tool, which parameters that are important to annotate and how to annotate them. All parameters are interpolated between user inputs.

Control

The “video player” has 6 keyboard controls:

- “W” to play
- “S” to pause
- “A” to go back one frame
- “D” to go forward one frame
- “Q” to quick backward
- “E” to quick forward

There are also software controls to do the same functions in the control button menu as seen in the figure below. Below the video player window is an infromation window that tells the user the current status of the program i.e what parameter is currently being input.

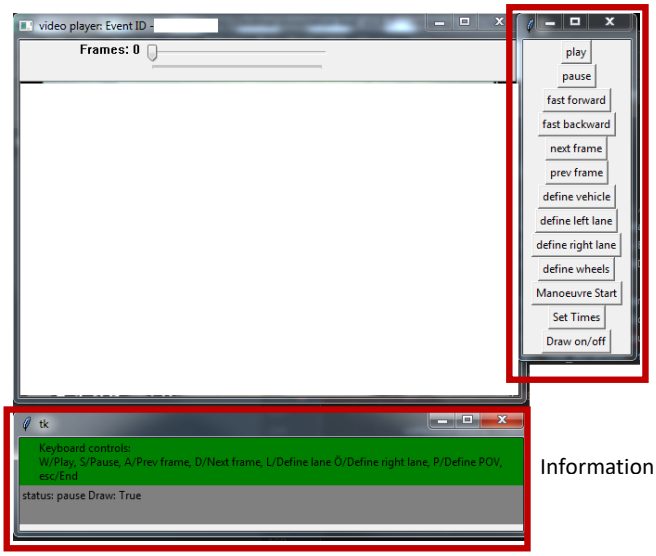

Control buttons

Information Window

In essence, there are 6 parameters:

1. POV placement (BOX)
2. POV wheels (two dots on the ground plane where the POV wheels touch the ground)
3. Left/right lanes (two or more dots on each lane)
4. Maneuver start (Frame number of the approximated start of maneuver)
5. Blinker start (frame number when the POV starts the indicator signal)
6. Lane cross (frame number where the POV crossed the lane marking of the SV lane)

1 POV placement

This is marked with a box around the POV rear. This box should be bounding the tail-light of the POV, since the POV pixel width is what is used to estimate its lateral and longitudinal placement relative to the camera on the SV. If the POV is further than approx 40m away, don't try to annotate it each frame, since it becomes harder and the output becomes noisy. Wait until the POV is at approx 20m before fine tuning the annotation. The tool output is displayed in the plots as a red-dotted line. These plots are used to compare the tool output to the radar range.

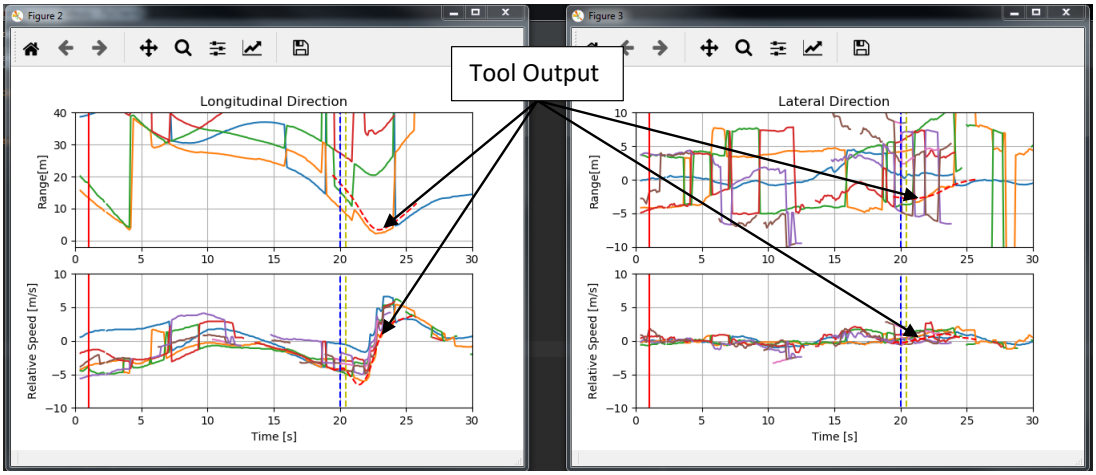

To draw this box do the following:

1. Click the "define vehicle" button
2. Use the mouse to draw a box around the rear of the vehicle
3. If you want to fine-tune the placement, there are keyboard controls to do so.
    a. To move the upper left corner of the box, use
        i. "W" to move up
        ii. "S" to move down
        iii. "A" to move left
        iv. "D" to move right
    b. To move the bottom right corner of the box, use the num-pad keys
        i. "8" to move up
        ii. "5" to move down
        iii. "4" to move left
        iv. "6" to move right

    Together, these simple controls should give you the ability to draw the box anywhere on the frame by moving it pixel by pixel. I usually have my left hand on the "wsad" keys and my right on the num-pad "8546" keys. After a couple of annotations you get used to it.

    c. To confirm a selection, press "Enter". The box color should change to green and the approximated distances should appear above the box in meters.
    d. To clear a selection, press "c"

After annotating the video, there are controls to improve the accuracy by changing:

- SV hood length: Changing this will remove the offset in the Longitudinal range
- Time-series offset: Changing this will shift the radar data and all timeservers data in time to account for the sync issue between the data and the video

2 POV wheels

The POV wheels are used to estimate the POV heading relative to the lane. To define these do the following:

1. Press the “define wheels” button
2. Use the mouse and click two time on the place where the POV wheel contact the ground
3. Press “Enter” key to confirm selection
4. Press “c” key to cancel selection

3 Left/Right lane marking

The lane markings are used to calculate the SV placement and heading in the lane. The SV heading is needed to calculate the POV heading as well. This means that to get a POV heading in a frame, you must have defined the left and right lanes and POV wheels.

To define the lanes, do the following:

1. Press “define left/right lane” separately
2. Use the mouse to place two or more dots on the lanes
3. Press “Enter” key to confirm selection
4. Press “c” key to cancel selection

4 Maneuver start

This parameter is just to make it easier for me to isolate the lane-change when I’m extracting the trajectory. This should be set last, after you have annotated the POV, wheels and lanes. This will appear on the plots as a vertical blue-dotted line. Define this at a time where the tool output is plotted.

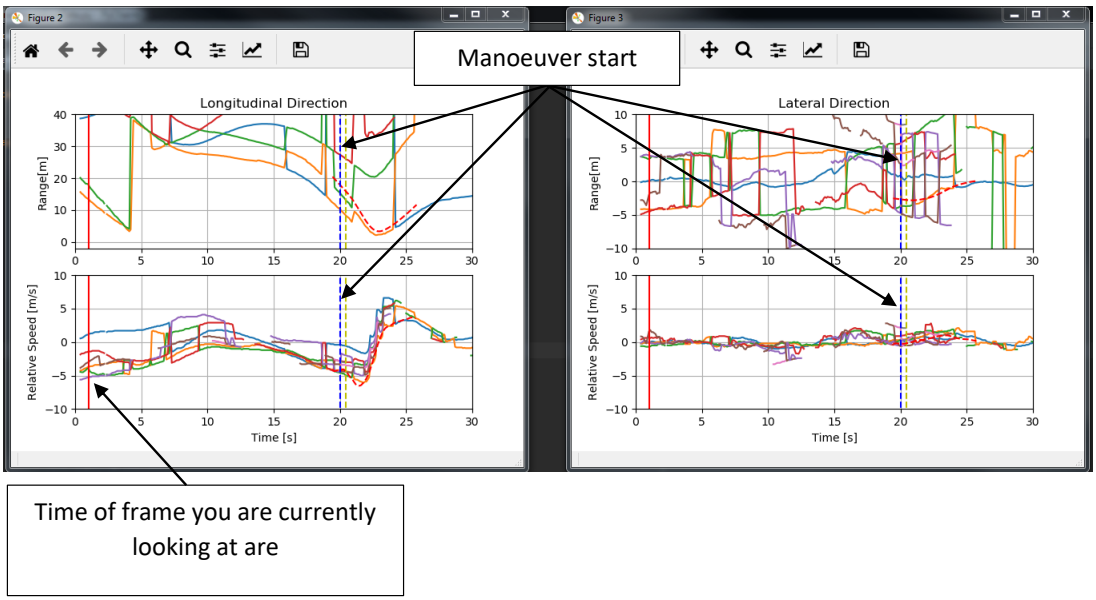

To define this, do the following:

1. Navigate to a frame where the tool output is defined
2. Press “manoeuver start”

5 Blinker start

This is the point in time where the POV starts signaling, if it ever does.

To define this do the following:

1. Navigate to the frame where the POV starts to indicate lane change, if ever
2. Press “set times” then “blinker start”

6 POV lane cross

This is the point in time where the POV crosses the lane.

To define this, do the following

1. Navigate to the frame where the POV crosses the lane
2. Press “set times” then “lane cross”